Charles University in Prague
Faculty of Mathematics and Physics

BACHELOR THESIS

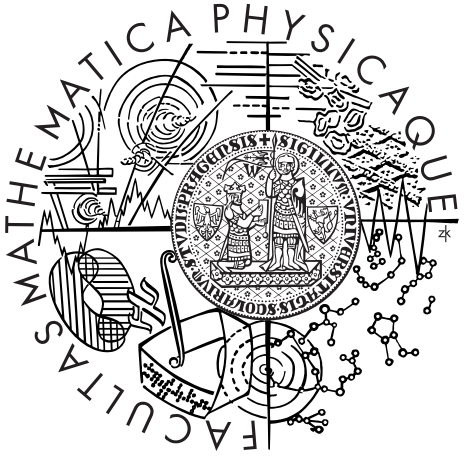

Lukáš Gráf

Model průchodu dvojitou bariérou s anharmonickými vibracemi

Model of transmition through double barrier with anharmonic vibrations

Institute of Theoretical Physics

Supervisor of the bachelor thesis: Martin Čížek

Study programme: Physics

Specialization: General Physics

Prague 2012

I would like to thank my supervisor, doc. Martin Čížek, for his methodical guidance, patience, time and overall help during the creation of this thesis.

I declare that I carried out this bachelor thesis independently, and only with the cited sources, literature and other professional sources.

I understand that my work relates to the rights and obligations under the Act No. 121/2000 Coll., the Copyright Act, as amended, in particular the fact that the Charles University in Prague has the right to conclude a license agreement on the use of this work as a school work pursuant to Section 60 paragraph 1 of the Copyright Act.

In ..... date ..... signature of the author

Název práce: Model průchodu dvojitou bariérou s anharmonickými vibracemi

Autor: Lukáš Gráf

Katedra: Ústav teoretické fyziky

Vedoucí bakalářské práce: doc. RNDr. Martin Čížek, Ph.D., Ústav teoretické fyziky

Abstrakt: V této práci se zabýváme elektronovým rozptylem na molekulárním můstku s anharmonickými vibracemi. Daný můstek modelujeme dvojitou bariérou obsahující kosinovou závislost na vibrační souřadnici. Průchod elektronu skrze bariéru si lze představit jakožto pohyb po povrchu nekonečně dlouhého válce s potenciální energií, která je nulová všude kromě omezené prostorové oblasti, v níž je dána pomocí deltafunkčních členů. Tento 2D problém řešíme jak metodou matice přechodu, tak užitím teorie rozptylu. Numericky přesnou pravděpodobnost průchodu elektronu dvojitou bariérou počítáme pomocí vlastního programu a studujeme její závislost na parametrech modelu. Jednotlivé parametrické režimy porovnáváme s různými aproximacemi, které lze pro dané nastavení použít. Elastický rozptyl aproximujeme jednodimenzionální a Chaseovou aproximací, zatímco vibrační excitaci srovnáváme s výsledky LCP aproximace. Získané grafy potvrzují správnost aproximačních metod hojně využívaných v molekulární fyzice.

Klíčová slova: kvantová teorie rozptylu, rezonance, elektronový transport

Title: Model of transmition through double barrier with anharmonic vibrations

Author: Lukáš Gráf

Department: Institute of Theoretical Physics

Supervisor: doc. RNDr. Martin Čížek, Ph.D., Institute of Theoretical Physics

Abstract: In the presented thesis we study the electron scattering off a molecular junction with anharmonic vibrations. This junction we simulate by a double barrier including the cosine dependence on the vibrational coordinate. The electron transmission through the barrier can be viewed as movement of the electron on the surface of infinitely long cylinder with zero potential energy everywhere except for a finite region where it is described by delta function terms. We solve this 2D problem employing the transfer matrix method and we present also the scattering theory approach to the problem. Using our own program we compute the numerically exact transmission probability and we investigate its dependence on parameters characterizing the model. We compare particular parametric regimes with various approximations which can be used for given settings. The elastic scattering is approximated by one-dimensional and Chase approximations whereas in case of vibrational excitation we employ the LCP approximation. Resulting graphs affirm that these approximation methods often used in molecular physics work very well.

Keywords: quantum scattering theory, resonances, electron transport

Contents

Introduction

The expansion of nanoscience in recent decades shows the way which modern technologies can take and even today nanotechologies play an important role in various fields. There are methods how to produce or control devices or material structures at nanometer scales; what is more, there even exist specialized research centers where they are able to operate objects with atomic scale accuracy.

Miniaturisation is undoubtedly one of the words which best characterize the development of technologies in the modern age. Looking back, the field where this trend is most apparent is probably the electronic industry. Although a few decades ago computers were the size of large halls nowadays there are laptops not bigger than a book consuming much less energy and providing us with incomparably higher computational power. The process of miniaturisation is in this field closely associated with the number of electronic components placed on a chip and therefore also with their size. It is obvious that this process will inevitably reach a limit at which the contemporary electronic structures stop working and completely new effects will have to be taken into account in their construction. Although employing the contemporary used methods it is not possible to produce components with atomic scale accuracy, there is another method which can do so, namely the chemical synthesis [1].

Designing of microscopic electronic components is the subject of active area of physics called *Molecular electronics*. The components are in this case represented by molecules that are specially constructed in order to have required properties. The process of the current transmission through the molecule is governed by quantum mechanics, which in consequence leads to a number of nontrivial problems.

First step is to investigate and describe the conductive characteristics of particular molecules. Experimentally, there are methods to link two macroscopic metal electrodes by a single molecule creating a *molecular junction*, which consequently enables us to measure the current flowing through it. However, complex theoretical description of such a process is very difficult. The molecules are often large and the geometry of their connection to the electrodes is mostly unknown. Additionally, we have to consider also the influence of molecular vibrations which can be significant for heat dissipations and decoherence [1].

One of the methods already developed for the description of the current flow through a molecular junction is the Landauer approach [2]. Basic idea of this approach is the fact that we can think of the current flow through the molecule as the electron transmission through the potential barrier. If we confine ourselves to elastic processes it is possible to derive an exact relation (*Laundauer formula*) for the calculation of the current flowing through the molecule

$$\mathcal{I} = \frac{e}{\pi\hbar} \int_{-\infty}^{+\infty} \left[f_L(E) - f_R(E) \right] \mathcal{T}(E) \mathrm{d}E, \tag{1}$$

where $\mathcal{T}(E)$ denotes the transmission probability of electron with energy E through the molecule and $f_{L,R}(E)$ is the Fermi-Dirac distribution corresponding to the left or the right electrode.

In this thesis we focus on the study of a simple but exactly solvable molecular junction with anharmonic vibrational degree of freedom. This kind of junction

can be represented for instance by a molecule of benzene which is linked to the electrodes by two opposite vertices, see Figure 1 which is reprinted here with permition from thesis of I. A. Pshenichnyuk [3]. The molecule with a rotational degree of freedom is in our model simulated by double potential barrier including cosine terms. In the first chapter we resume the problem of the simple one-dimensional double barrier introducing the formalism of quantum scattering theory. The second chapter contains the solution of the full inelastic model using the tranfer matrix method and its connection to the scattering theory approach. In the last chapter we present the results obtained from the exact solution described in the second chapter and we compare it with various approximation methods. We also try to give interpretation of some features observed in calculated transmission functions.

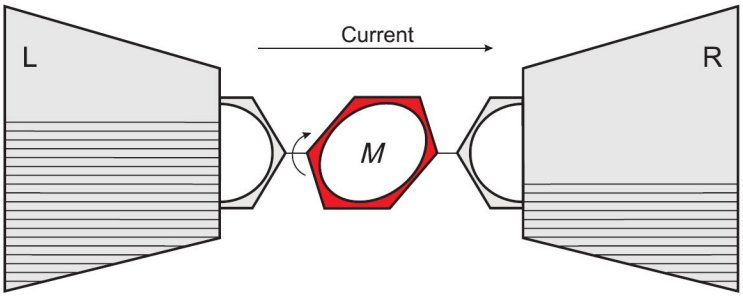

Figure 1: A schematic illustration of the molecular junction formed by a benzene molecule.

1. Double delta function potential barrier

The aim of this thesis is to solve the problem of double barrier with anharmonic vibrations. Therefore our model will include two degrees of freedom - electronic and vibrational. Before we proceed to the solution of the barrier including the vibrational degree of freedom let us start with a short summary of the elementary problem of tunneling through the double delta function potential barrier in one dimension.

Generally, there exist more ways how to calculate the transmission through a double barrier. In this work we will be concerned especially with the method of the transfer matrix (which uses the knowledge of the general solution of the Schrödinger equation, [4]) and the scattering theory approach. The former method which consists in familiar matching of wave functions and their derivatives at boundaries of particular parts of space is more straightforward whereas the latter can give us more insight into the problem exploiting the sophisticated scattering theory formalism. As we will see this approach is worth in particular when dealing with more complicated problems.

1.1 Theoretical background and solution

The transmission coefficient of the particle that scatters off the two delta potential barriers can be obtained without making much effort by the transfer matrix method mentioned above. However, for the further development it will be convenient to solve this problem using the scattering theory formalism with whose principles we will get acquainted at the same time.

We start with expressing the Hamiltonian of the problem we are about to solve, that is

$$H = \frac{p^2}{2M} + V(x), \tag{1.1}$$

where $p = -i\hbar\frac{\partial}{\partial x}$ is the momentum operator and whole the first term represents the kinetic energy of the electron transmitting through the barrier $V(x)$. Without loss of generality by choice of proper units we will in further development always set for simplicity $\hbar = M = 1$ (M is the electron mass).

As for the potential double barrier $V(x)$, we assume the case when the first barrier is located at $x = -a$ and the second at $x = a$ symmetrically with respect to the coordinate origin, thus the potential reads

$$V(x) = \alpha_L\delta(x + a) + \alpha_R\delta(x - a).$$

Here the a again is not a free parameter and by changing the units we can set $a = 1$ rescaling α_L, α_R properly. Although further in this text we will for lucidity still keep this constant, its value will be always set to 1.

In general, the scattering process can be described as follows. An incident state $|\psi_{in}\rangle$ (*in* asymptote) of the particle is an eigenstate of the free particle Hamiltonian H_0. We assume that the particle is initially distant enough from the

barrier so it does not feel the potential. When it gets closer to the potential V it is scattered resulting in the state $|\psi\rangle$ which is an eigenstate of the full Hamiltonian $H = H_0 + V$. As the particle moves far from the scattering center it again behaves freely, this asypmtotic state (*out* asymptote) we denote $|\psi_{out}\rangle$. It can be shown that for each asymptote $|\psi_{in}\rangle$ there exists an appropriate state $|\psi\rangle$. It is convenient to choose the in asymptote as a plane waves with certain momentum. Denoting a plane wave with a wave vector k as $|\psi_k\rangle$ we can write $|\psi_{in}\rangle = |\psi_k\rangle$.

If we express the state $|\psi\rangle$ as the sum of the free and the scattered state $|\psi\rangle = |\psi_{in}\rangle + |\psi_{sc}\rangle$ and introduce this sum into the Schrödinger equation for state $|\psi\rangle$ we can derive the following expression

$$|\psi_{sc}\rangle = (E + i\varepsilon - H_0)^{-1} V |\psi\rangle ,$$

where ε is an infinitesimally small number added to E in order to ensure that the operator inversion exists. The operator $(E + i\varepsilon - H_0)^{-1}$ is the well-known unperturbed Green operator $G_0^{(+)}$ and the scattered state satisfies the outgoing boundary condition

$$\lim_{|x|\to+\infty} |\psi_{sc}\rangle = \frac{1}{\sqrt{2\pi}} e^{ik|x|}.$$

Hence, after adding $|\psi_{in}\rangle$ to the derived expression for $|\psi_{sc}\rangle$ we can write

$$|\psi\rangle = |\psi_{in}\rangle + G_0^{(+)} V |\psi\rangle ,$$

which is the well-known *Lippmann-Schwinger equation.*

Let us now apply this equation to our problem. First we write the Lippman-Schwinger equation in the coordinate representation

$$\psi(x) = \psi_{in}(x) + \int G_0^{(+)}(x, x') V(x') \psi(x') \mathrm{d}x,$$

in which we can put our potential. After the integration we obtain

$$\psi(x) = \psi_{in}(x) + \alpha_L G_0^{(+)}(x, -a)\psi(-a) + \alpha_R G_0^{(+)}(x, a)\psi(a).$$

Considering this equation at $x = -a$ and $x = a$ we get the system of two equations for $\psi(-a)$ and $\psi(a)$, which can be easily solved to obtain the expressions for the wave function evaluated at these two points. Additionally, we know that the Green function $G_0^{(+)}$ corresponding to the free particle in one dimension has in the x-representation the following form

$$G_0^{(+)}(x, x') = \lim_{\varepsilon\to 0} \frac{1}{2\pi} \int_{-\infty}^{+\infty} \frac{e^{ik'(x-x')}}{E - E_k + i\varepsilon} \mathrm{d}k' = \frac{1}{ik} e^{ik|x-x'|}, \tag{1.2}$$

where $E_{k'} = \frac{k'^2}{2}$. Hence, we can derive the expression for $\psi(x)$

$$\psi(x) = \frac{e^{ikx}}{\sqrt{2\pi}} - \frac{i\alpha_L e^{ik(|x+a|-a)} \left(k + i\alpha_R \left(1 - e^{4ika}\right)\right) - ik\alpha_R e^{ik(|x-a|+a)}}{\sqrt{2\pi}\left(k^2 + ik\left(\alpha_L + \alpha_R\right) - \alpha_L\alpha_R\left(1 - e^{4ika}\right)\right)}. \tag{1.3}$$

In scattering theory it is very useful to define another operator, namely the *T-operator.* It can be written in terms of the full Green operator $G^+(E) = (E + i\varepsilon - H)^{-1}$ as

$$T(z) = V + VG^+(z)V. \tag{1.4}$$

Using again the denotation $|\psi_k\rangle = e^{ikx}$ the expression

$$\langle\psi_{k'}|\, T(z)\, |\psi_k\rangle \tag{1.5}$$

represents so called *off-shell* T matrix. Nevertheless, for descriptions of one particle collisions the *on-shell* elements of the T matrix are only needed

$$T(k',k) = \lim_{\varepsilon\to 0} \langle\psi_{k'}|\, T\left(E_k + i\varepsilon\right) |\psi_k\rangle\,. \tag{1.6}$$

It means that the on-shell elements of the T matrix are the $k',\ k$ matrix elements of $T(z)$ for $z = E_k + i0$ and $E_{k'} = E_k$.

In the scattering theory framework another expression for the on-shell T matrix [5] is usually derived

$$T(k',k) = \langle\psi_{k'}|\, V\, |\psi\rangle\,. \tag{1.7}$$

This is precisely the relation of our interest because we have already calculated the full wave function $\psi(x)$.

Knowledge of the on-shell T matrix elements alone determines the scattering operator S which can be understood as a map between the *in* and *out* asymptotes, i.e. it holds $|\psi_{out}\rangle = S\,|\psi_{in}\rangle$. Its relation to $T(k',k)$ is

$$\langle\psi_{k'}|\, S\, |\psi_k\rangle = \delta(k'-k) - 2\pi i\delta(E_{k'} - E_k)T(k',k). \tag{1.8}$$

Once we express T and S matrices of a particular problem, it is easy to determine the transmission and reflection probabilities P_T, P_R. The energy conservation law requires that k' acquires only two values $\pm k$ hence we write

$$T_+ = \langle\psi_{+k}|\, T\, |\psi_k\rangle = \langle\psi_{+k}|\, V\, |\psi\rangle\,, \tag{1.9}$$

$$T_- = \langle\psi_{-k}|\, T\, |\psi_k\rangle = \langle\psi_{-k}|\, V\, |\psi\rangle\,. \tag{1.10}$$

Then the transmission and reflection probabilities are defined as

$$P_T = \left| I - \frac{2\pi i}{k} T_+ \right|^2, \tag{1.11}$$

$$P_R = \frac{(2\pi)^2}{k^2}\, |T_-|^2\,. \tag{1.12}$$

We can compare these relations with the more familiar 3D potential scattering. There we introduce a quantity closely related to the on-shell T matrix, namely the *scattering amplitude* f which is defined as

$$f(k',k) = -(2\pi)^2 m T(k',k). \tag{1.13}$$

Based on the scattering amplitude we calculate the *differential cross section* $\frac{\mathrm{d}\sigma}{\mathrm{d}\Omega}$ since it can be shown [5] that

$$\left(\frac{\mathrm{d}\sigma}{\mathrm{d}\Omega}\right)(k',k) = |f(k',k)|^2\,. \tag{1.14}$$

This well-known expression describes the probability density that the particle emerges scattered into a certain direction. In one-dimensional problem it is possible to define the scattering amplitude analogously as

$$f(k',k) = -\frac{2\pi i}{k} T(k',k) \tag{1.15}$$

and instead of the cross section we have the reflection probability defined above.

In our case of the double delta potential barrier the two on-shell matrix elements of the T matrix are (subst. 1.3 in 1.7)

$$T_+ = \frac{ik}{2\pi}\left(\frac{\alpha_L\alpha_R\left(1-e^{4ika}\right)-ik\left(\alpha_L+\alpha_R\right)}{k^2+ik\left(\alpha_L+\alpha_R\right)-\alpha_L\alpha_R\left(1-e^{4ika}\right)}\right), \tag{1.16}$$

$$T_- = \frac{ik}{2\pi}\left(\frac{\alpha_L\alpha_R\left(e^{-2ika}-e^{2ika}\right)-ik\left(\alpha_L e^{-2ika}+\alpha_R e^{2ika}\right)}{k^2+ik\left(\alpha_L+\alpha_R\right)-\alpha_L\alpha_R\left(1-e^{4ika}\right)}\right). \tag{1.17}$$

To complete the theoretical background, there is also another important information contained in the S matrix. Within the frame of scattering theory it can be shown that the poles of the $S(k)$ matrix as a complex function of the wave vector k correspond for $\{\mathrm{Im}(k) < 0\}$ to *resonances*, the striking phenomena which can be observed not only in atomic but also in nuclear and particle physics. In 3D scattering, resonances result in sharp peaks in the energy dependence of the cross section therefore (in our case) they lead to the peaks in energy dependence of the transmission probability. If we express the S matrix as a function of energy then its pole at $\tilde{E} = E_r - \frac{i\Gamma}{2}$ close to the real axis implies that in the graph of the transmission probability as a function of energy we can observe the peak of width Γ positioned at E_r.

1.2 Results

Using the expressions for the wave function ψ and for the T matrix corresponding to the double delta barrier problem (which we have derived above) we can now easily write the transmission and reflection probabilities as

$$P_T = \left|\frac{1}{k^2+ik(\alpha_L+\alpha_R)-\alpha_L\alpha_R(1-e^{4ika})}\right|^2, \tag{1.18}$$

$$P_R = \left|\frac{\alpha_L\alpha_R\left(e^{-2ika}-e^{2ika}\right)-ik\left(\alpha_L e^{-2ika}+\alpha_R e^{2ika}\right)}{k^2+ik\left(\alpha_L+\alpha_R\right)-\alpha_L\alpha_R\left(1-e^{4ika}\right)}\right|^2. \tag{1.19}$$

Graph of the transmission and reflection probabilities as functions of energy $E = \frac{k^2}{2}$ of the incoming particle is for symmetric double barrier displayed in Fig. 1.1. Both barriers are chosen to have the height $\alpha_L = \alpha_R = 5$. We can see that the depicted resonance peaks are sharp which is caused by the fact that the barriers are high. Additionally, in this case the transmission resonance peaks reach the value 1. On the contrary, the peaks in the graph in Fig. 1.2 describing the transmission and reflection probabilities related to the asymmetric double barrier do not reach the value 1, they are evidently lower. This effect is caused purely by the asymmetry of the double barrier.

The expressions 1.18, 1.19 that we have derived above satisfy the condition $P_T + P_R = 1$, which is also obvious from the corresponding graphs. This relatively apparent result stating that the particle simply cannot disappear is equivalent to the unitarity of the S matrix, which can be formally proved [5].

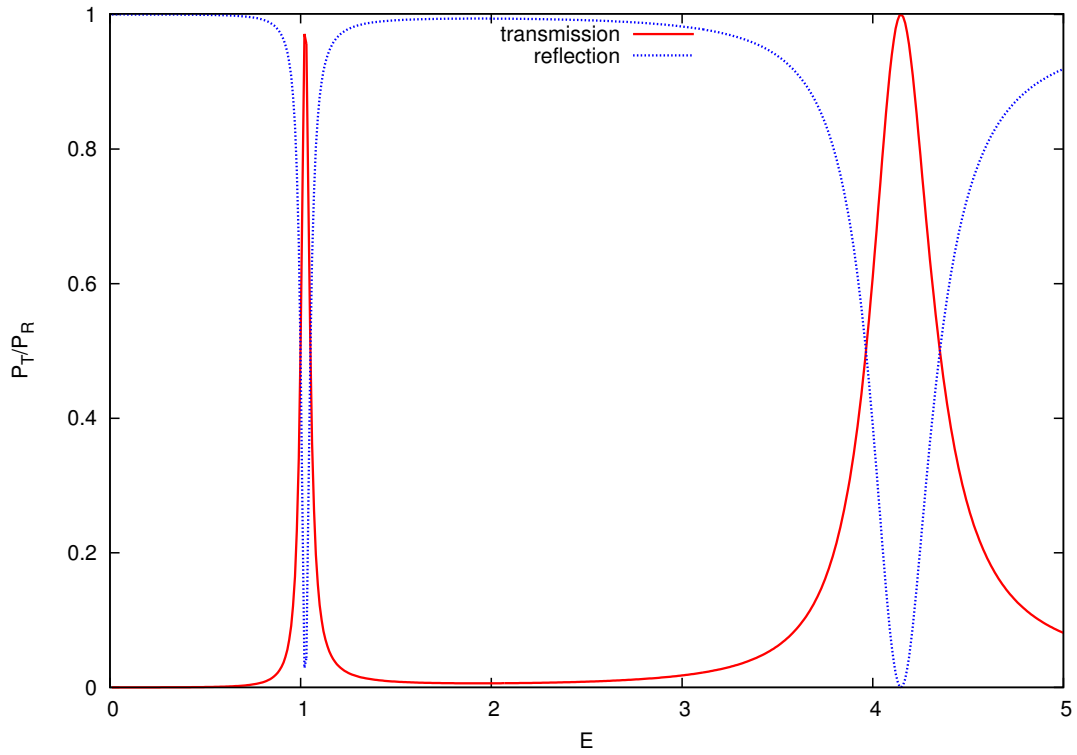

Figure 1.1: Graph of the energy dependence of the transmission (P_T) and reflection (P_R) probabilities for symmetric double delta function potential barrier. Prefactors of both delta functions are equal $\alpha_L = \alpha_R = 5$. It is obvious that the identity $P_T + P_R = 1$ is fulfilled.

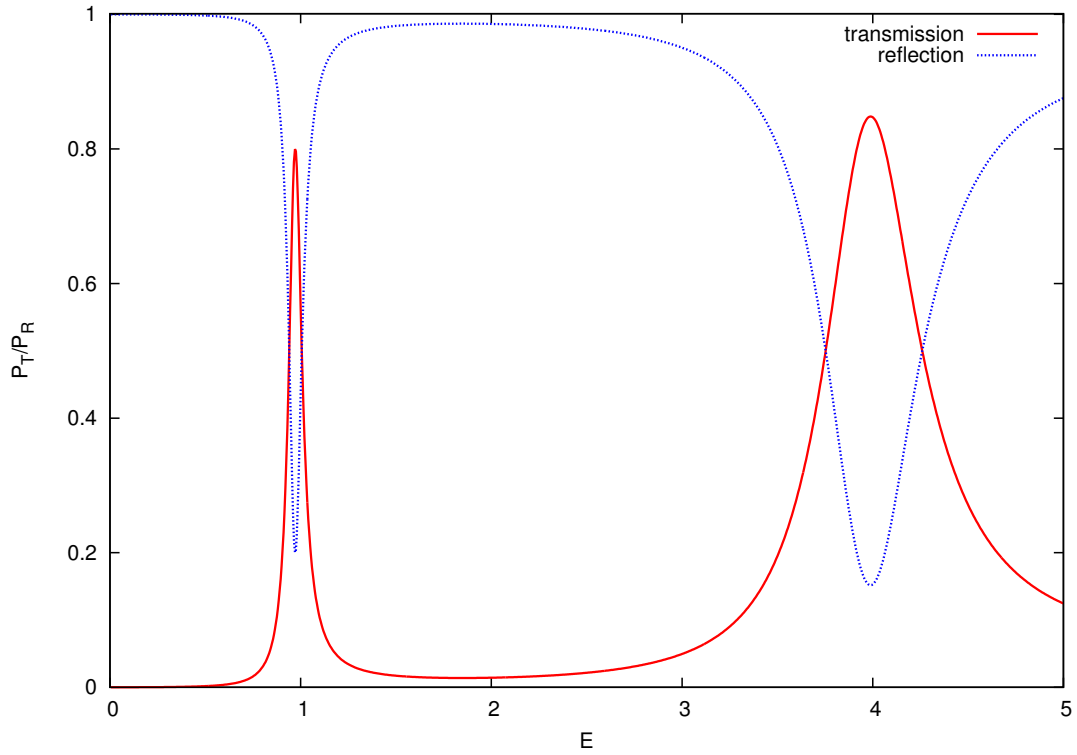

Figure 1.2: This graph describes the transmission (P_T) and reflection (P_R) probabilities for asymmetric double delta function potential barrier. Prefactors of particular delta functions are $\alpha_L = 5$ and $\alpha_R = 3$.

2. Double delta barrier with anharmonic vibrations

Now we focus on the model of electron transmission through the molecular junction with rotational degree of freedom. In this case we deal with a two-dimensional problem where the first coordinate x is linear and specifies the position of the particle (electron), whereas the second coordinate φ is angular and describes the orientation of the bridging molecule. Such a problem can be mapped to motion of one particle in two-dimensional potential characterizing the molecular junction. To be more specific, we can simulate the junction by the potential barrier involving cosine terms dependent on the angular variable φ. The transmitting electron therefore experiences the potential barrier with strength determined by the orientation of the molecule.

2.1 Solution using the transfer matrix method

In the first part we calculate the transmission through such a barrier relatively straightforwardly deriving the transfer matrix for this problem. In the second part of the solution we demonstrate that the scattering theory approach gives the same results and it provides us with a powerfull framework suitable for description and analysis of all the related physical processes.

The Hamiltonian of the described system is

$$H = \frac{p^2}{2} + \frac{\Pi^2}{2I} + \lambda_L(\varphi)\delta(x+a) + \lambda_R(\varphi)\delta(x-a). \tag{2.1}$$

The first term is the kinetic energy of electron, $p^2 = -\frac{\partial^2}{\partial x^2}$. The second term represents the molecular kinetic energy, $\Pi^2 = -\frac{\partial^2}{\partial \varphi^2}$. The first two terms together constitute the free Hamiltonian H_0. Remaining two terms represent the potentials corresponding to the left and to the right barrier.

As well as in the previous elementary problem we assume the symmetric position of the barriers localized at $x = -a$ and $x = a$. However, now both of them consist not only of the term representing the fixed delta function potential barrier but also of the term corresponding to the delta function potential with the rotational degree of freedom. Therefore λ_L and λ_R now are not constant. They depend on the coordinate φ and this dependence is responsible for the molecular excitations.

To set up the model we choose the cosine dependence of $\lambda_L(\varphi)$ and $\lambda_R(\varphi)$ to mimic the behaviour of real molecules [3]. Hence, at $x = -a$ the potential reads

$$\lambda_L(\varphi) = \alpha_L + \beta_L \cos(\varphi) = \alpha_L + \frac{\beta_L}{2}\left(e^{i\varphi} + e^{-i\varphi}\right), \tag{2.2}$$

whereas at $x = a$ the potential equals to

$$\lambda_R(\varphi) = \alpha_R + \beta_R \cos(\varphi - \varphi_0) = \alpha_R + \frac{\beta_R}{2}\left(e^{i(\varphi-\varphi_0)} + e^{-i(\varphi-\varphi_0)}\right). \tag{2.3}$$

As seen the left potential barrier differs from the the right one by the factor $e^{i\varphi_0}$ determining the relative orientation between the two rotational barriers. Constants α_L, β_L, α_R and β_R are real and they determine the "height" of particular potential barriers. Although in all relations and derivations we use the constants α and β with the subscripts L and R distinguishing the left and the right barriers to keep the generality of the problem, when plotting the results for particular values of parameters in the next chapter we will for simplicity always assume $\alpha_L = \alpha_R \equiv \alpha$ and $\beta_L = \beta_R \equiv \beta$. Also in all the discussions we will use just the denotation α and β without the subscripts.

The double barrier divides the x-axis into three parts $(-\infty, -a)$, $(-a, a)$ and (a, ∞) in which the two-dimensional Schrödinger equation for a free particle holds. Hence, we know that the solution with energy E can be expressed in every region as a superposition of eigenstates $|k, m\rangle \equiv |\psi_k\rangle\,|\phi_m\rangle$ of the free Hamiltonian H_0 with energy

$$E = \frac{k^2}{2} + \frac{m^2}{2I}. \tag{2.4}$$

Coefficients related to particular basis wave functions can be determined applying the boundary conditions. In general, we can write the equations that impose the continuity of ψ and $\frac{d\psi}{dr}$ at $x = -a$ and $x = a$ as follows

$$\psi_+(x,\varphi) = \psi_-(x,\varphi), \tag{2.5}$$

$$\frac{\mathrm{d}}{\mathrm{d}x}\psi_+(x,\varphi) - \frac{\mathrm{d}}{\mathrm{d}x}\psi_-(x,\varphi) = \lambda(\varphi)\psi(x,\varphi), \tag{2.6}$$

where $\psi_{+,-}$ are the wave functions on the right side or the left side of the barrier and the potential $\lambda(\varphi)$ stands for $\lambda_R(\varphi)$ or $\lambda_L(\varphi)$ in case of the right or the left barrier.

The equations 2.5, 2.6 we express for particular barriers, expand them in the eigenbasis $|k, m\rangle$ and then we project them onto the Fourier basis functions $|\phi_m\rangle = \frac{1}{\sqrt{2\pi}} e^{im\varphi}$, $m \in \{-n, \ldots, -1, 0, 1, \ldots, n\}$ describing the angular degree of freedom. Of course, the index m should run from $-\infty$ to ∞, however, for our computation we can cut it off. To get precise results it is sufficient to take the n big enough, typically we choose $n = 100$. Every basis vector $|\phi_m\rangle$ corresponds to the vibrational kinetic energy $E_m = \frac{m^2}{2I}$ (I is the molecular moment of inertia). Introducing the shorthand notation $z_m = e^{ik_m a}$ we obtain for the wave functions at $x = -a$ following conditions

$$\delta_{mm_i} z_m^{-1} + r_m z_m = a_m z_m^{-1} + b_m z_m, \tag{2.7}$$

$$\begin{aligned}\left[a_m i k_m z_m^{-1} - b_m i k_m z_m\right] - \left[\delta_{mm_i} i k_m z_m^{-1} - r_m i k_m z_m\right] \\ = \beta_L \left[b_{(m+1)} z_{m+1} + b_{(m-1)} z_{m-1}\right] + 2\alpha_L \left[a_m z_m^{-1} \right. \\ \left. + b_m z_m\right] + \beta_L \left[a_{(m+1)} z_{m+1}^{-1} + a_{(m-1)} z_{m-1}^{-1}\right],\end{aligned} \tag{2.8}$$

where r_m are the coefficients of the reflected waves going to $-\infty$, wheareas a_m are the coefficients of the waves which have tunneled through the first barrier and which go to the right. Prefactors b_m relates to the left going waves reflected off the second barrier. The wave vectors pertaining to the individual base wave functions we denote as k_m.

Similarly at $x = a$ we have

$$a_m z_m + b_m z_m^{-1} = \tau_m z_m + 0_m z_m^{-1}, \tag{2.9}$$

$$\begin{aligned}\left[\tau_m i k_m z_m + 0_m i k_m z_m^{-1}\right] - \left[a_m i k_m z_m - b_m i k_m z_m^{-1}\right] \\ = \beta_R e^{-i\varphi_0}\left[\tau_{(m+1)} z_{m+1} + 0_{(m+1)} z_{m+1}^{-1}\right] + 2\alpha_L\left[\tau_m z_m \right. \\ \left. + 0_m z_m^{-1}\right] + \beta_R e^{i\varphi_0}\left[\tau_{(m-1)} z_{m-1} + 0_{(m-1)} z_{m-1}^{-1}\right],\end{aligned} \tag{2.10}$$

where τ_m are the coefficients of the waves transmitted through the double barrier and we assume that there are no left going waves in the third region.

Wave vectors k_m can be determined from the energy conservation law. Applying the free Hamiltonian on its eigenvector $|k, m\rangle$ we obtain

$$H_0 |k, m\rangle = (E_k + E_m) |k, m\rangle = \left(\frac{k_m^2}{2} + \frac{m^2}{2I}\right) |k, m\rangle, \tag{2.11}$$

therefore the wave vectors can be calculated as

$$k_m = \sqrt{2E - \frac{m^2}{I}}, \tag{2.12}$$

where E is the total energy of the system. In case $E_m > E$, the particular vibrational energy is not allowed and we say that *the m-th channel is closed*. Naturally, m's for which $E_m < E$ determine *open channels*.

The equations 2.7, 2.8 and 2.9, 2.10 we can rewrite in the matrix form that can be expressed schematically as

$$M_1 \begin{pmatrix} in \\ r \end{pmatrix} = M_2 \begin{pmatrix} a \\ b \end{pmatrix}, \tag{2.13}$$

$$M_3 \begin{pmatrix} a \\ b \end{pmatrix} = M_4 \begin{pmatrix} \tau \\ 0 \end{pmatrix}, \tag{2.14}$$

where the columns represent $(2n + 1)$-dimensional vectors containing the coefficients of the particular wave functions

$$\begin{pmatrix} in \\ r \end{pmatrix} = \left(\begin{array}{c} 0 \\ \vdots \\ 1 \\ \vdots \\ 0 \\ \hline r_{-m} \\ \vdots \\ r_0 \\ \vdots \\ r_m \end{array}\right), \quad \begin{pmatrix} a \\ b \end{pmatrix} = \left(\begin{array}{c} a_{-m} \\ \vdots \\ a_0 \\ \vdots \\ a_m \\ \hline b_{-m} \\ \vdots \\ b_0 \\ \vdots \\ b_m \end{array}\right), \quad \begin{pmatrix} \tau \\ 0 \end{pmatrix} = \left(\begin{array}{c} \tau_{-m} \\ \vdots \\ \tau_0 \\ \vdots \\ \tau_m \\ \hline 0 \\ \vdots \\ 0 \\ \vdots \\ 0 \end{array}\right). \tag{2.15}$$

The matrices M_i are block matrices

$$M_i = \left(\begin{array}{c|c} B_1 & B_2 \\ \hline B_3 & B_4 \end{array}\right), \tag{2.16}$$

where the blocks are formed by diagonal or maximally tridiagonal (lower blocks of the matrices M_2 and M_4) matrices.

The transfer matrix X, which tells us about the reflection and transmission characteristics of the potential barrier, is defined as

$$\begin{pmatrix} in \\ r \end{pmatrix} = X \begin{pmatrix} \tau \\ 0 \end{pmatrix}, \tag{2.17}$$

thus from equations 2.13, 2.14 we obtain

$$X = M_1^{-1} M_2 M_3^{-1} M_4. \tag{2.18}$$

The inversion of the matrices M_1 and M_3 can be easily calculated analytically because all their blocks are diagonal.

Now it is obvious that also the transfer matrix has in this case the form of a block matrix

$$X = \left(\begin{array}{c|c} X_1 & X_2 \\ \hline X_3 & X_4 \end{array} \right), \tag{2.19}$$

where the block X_1 connects initial and transmission coefficients

$$\begin{pmatrix} \tau_{-m} \\ \vdots \\ \tau_0 \\ \vdots \\ \tau_m \end{pmatrix} = X_1^{-1} \begin{pmatrix} 0 \\ \vdots \\ 1 \\ \vdots \\ 0 \end{pmatrix}. \tag{2.20}$$

Thus it is obvious that if we want to extract the transmission coefficients we are interested in the inversion of the first block of the matrix X. The block X_1 is in fact five-diagonal matrix. To invert this matrix analytically would be very painful and probably worthless. Therefore we have calculated the inversion numerically in Fortran utilizing the method of *LU decomposition* which was adopted from [6] and modified in order to work with complex matrices.

Using the obtained coefficients τ_m we can calculate also the reflection coefficients r_m, it holds

$$\begin{pmatrix} r_{-m} \\ \vdots \\ r_0 \\ \vdots \\ r_m \end{pmatrix} = X_3 \begin{pmatrix} \tau_{-m} \\ \vdots \\ \tau_0 \\ \vdots \\ \tau_m \end{pmatrix}. \tag{2.21}$$

Having computed the coefficients τ_m and r_m we can easily derive the reflection and transmission probabilities comparing the incoming and outcoming probability flux. Thereby the probabilities $P^R_{mm_i}$ and $P^T_{mm_i}$ that the electron in the initial state m_i is reflected off or transmitted through the barrier resulting in the state m are given by following relations

$$P^R_{mm_i} = \frac{k_m}{k_{m_i}} \left| r_m \right|^2, \; P^T_{mm_i} = \frac{k_m}{k_{m_i}} \left| \tau_m \right|^2. \tag{2.22}$$

The total reflection probability P_R and the total transmission probability P_T we obtain as the sum over all possible outcoming states

$$P_R = \sum_m \left(\frac{k_m}{k_{m_i}} \, |r_m|^2 \right), \; P_T = \sum_m \left(\frac{k_m}{k_{m_i}} \, |\tau_m|^2 \right). \tag{2.23}$$

The subscript m here runs only over the indices corresponding to the open channels. For all the closed channels $P_{mm_i} = 0$ by definition.

2.2 Scattering theory context

Once we have solved the problem using the transfer matrix we can perform in short the scattering theory approach and compare both methods. That will allow us afterwards to employ the scattering theory framework in order to get a better physical insight into the problem.

We proceed similarly as in the solution of the one-dimensional problem in the first chapter. We start again with the Lippmann-Schwinger equation

$$|\psi\rangle = |\psi_{in}\rangle + G_0 V \, |\psi\rangle \, , \tag{2.24}$$

however, currently the wave function depends also on φ so it can be expanded in the eigenbasis $|k, m\rangle$ of the free Hamiltonian H_0 as mentioned above. The initial state we can consequently write as $|\psi_{in}\rangle = |k_i, m_i\rangle$. Similarly as in the transfer matrix method we project the equation onto the Fourier basis $|\phi_m\rangle$, $m \in \{-n, \ldots, -1, 0, 1, \ldots, n\}$, that is

$$\langle m|\psi\rangle = \delta_{mm_i} \, |k_i\rangle + \langle m| \, G_0 \, |m'\rangle \, \langle m'| \, V \, |\psi\rangle \, . \tag{2.25}$$

Using the scattering theory language we currently solve a multichannel problem where every m relates to a single channel.

The Green operator G_0 projected onto the angular basis has in the x representation the form of diagonal matrix

$$\langle k, m| \, G_0 \, |k', m'\rangle = \frac{\delta_{mm'}}{ik_m} e^{ik_m|x-x'|}. \tag{2.26}$$

Equation 2.25 represents a system of $(2n+1)$ equations which can be naturally written in the matrix form. Evaluating the set of equations at points $x = \pm a$ we deal with two matrix equations which can be schematically written as one large matrix equation

$$\begin{pmatrix} \Psi(-a) \\ \Psi(a) \end{pmatrix} = \begin{pmatrix} \Psi_{in}(-a) \\ \Psi_{in}(a) \end{pmatrix} + \left[\frac{1}{ik} \begin{pmatrix} \Lambda_L & z^2\Lambda_R \\ z^2\Lambda_L & \Lambda_R \end{pmatrix} \right] \begin{pmatrix} \Psi(-a) \\ \Psi(a) \end{pmatrix}, \tag{2.27}$$

where we introduced the projections of the potentials onto the angular basis, namely $\Lambda_{L,R} = \langle \phi_m| \, \lambda_{L,R}(\varphi) \, |\phi_{m'}\rangle$, whereas z and k are diagonal matrices with elements z_m and k_m at corresponding positions. Next important thing is that $\Psi(\pm a)$ denotes the $(2n+1)$-dimensional vector with components

$$(\Psi(\pm a))_m = \psi_m(\pm a) = \frac{1}{\sqrt{2\pi}} z_m^{\pm 1} \tag{2.28}$$

and, eventually, Ψ_{in} is the initial asymptotic state represented by the $(2n+1)$-dimensional vector with just i-th nonzero component which equals to

$$(\Psi_{in}(\pm a))_{m_i} = \psi_{m_i}(\pm a) = \frac{1}{\sqrt{2\pi}} z_{m_i}^{\pm 1}. \tag{2.29}$$

We again use the shorthand notation $z_m = e^{ik_m a}$.

Expressing the demanded vectors of unknown wave functions $\Psi(\pm a)$ from the equation 2.27 we get

$$\begin{pmatrix} \Psi(-a) \\ \Psi(a) \end{pmatrix} = \left[\begin{pmatrix} I \\ I \end{pmatrix} - \frac{1}{ik} \begin{pmatrix} \Lambda_L & z^2 \Lambda_R \\ z^2 \Lambda_L & \Lambda_R \end{pmatrix} \right]^{-1} \begin{pmatrix} \Psi_{in}(-a) \\ \Psi_{in}(a) \end{pmatrix}. \tag{2.30}$$

It is apparent that we are now facing a similar problem as in the transfer matrix method, that is we have to invert the matrix above in order to determine the functions $\psi_m(\pm a)$ which we need for the following computation of the *on-shell* T matrix. Using analogous relations as in the one-dimensional problem in the first chapter we obtain

$$T^+_{mm_i} = \frac{1}{\sqrt{2\pi}} \sum_{m'} \left[e^{ik_m a} \Lambda^L_{mm'} \psi_{m'}(-a) + e^{-ik_m a} \Lambda^R_{mm'} \psi_{m'}(a) \right], \tag{2.31}$$

$$T^-_{mm_i} = \frac{1}{\sqrt{2\pi}} \sum_{m'} \left[e^{-ik_m a} \Lambda^L_{mm'} \psi_{m'}(-a) + e^{ik_m a} \Lambda^R_{mm'} \psi_{m'}(a) \right]. \tag{2.32}$$

Now we can express the transmission probability which is in the multichannel problem described by relation

$$P^T_{mm_i} = \frac{k_m}{k_{m_i}} \left| \delta_{mm_i} - \left(\frac{2\pi i}{k_m} \right) T^+_{mm_i} \right|^2 = \left| \delta_{mm_i} - \left(\frac{2\pi i}{\sqrt{k_m k_{m_i}}} \right) T^+_{mm_i} \right|^2, \tag{2.33}$$

whereas the reflection probability is

$$P^R_{mm_i} = \frac{k_m}{k_{m_i}} \left| \left(\frac{2\pi i}{k_m} \right) T^-_{mm_i} \right|^2 = (2\pi)^2 \left| \frac{T^-_{mm_i}}{\sqrt{k_m k_{m_i}}} \right|^2. \tag{2.34}$$

For the total probabilities again the equalities 2.23 hold.

3. Results and discussion

In our model there are three main parameters which cannot be eliminated by the choice of units. It is the moment of inertia I and the constants α and β characterizing the height of the particular barriers. Another free parameter is, of course, the angle φ_0 setting the orientation of the molecule but it does not influence the behaviour of the model so significantly. Let us now discuss the choice of the values of the three important parameters I, α and β.

Since we have transformed the electron mass and the distance between the barriers so that these constants were equal to unity we in fact measure all the masses and distances in the units of m_e and a. The gap separating the left barrier from the right one is in reality typically several Bohr radii. The effective mass of the electron in a conductor is for standard materials in the range from 0.1 to 10 m_e but in *heavy fermion systems* it can reach up to 1000 m_e. The characteristic group that can rotate in a molecular junction is the methyl group CH_3 or the benzene molecule C_6H_6. Therefore the typical values of I are between 10^3 and 10^6. In case we consider heavy fermion systems the moment of inertia has a value from 10^0 to 10^6.

The constants α and β that scale the potential barriers have dimension of length times energy. This fact corresponds very well to the concept of a molecule caught in insulator between two conductors. The energy equals to the work function of the conductor and the length is the distance between the barriers. Since we can choose this distance the parameter α can be equal to arbitrary values but a reasonable order of magnitude of its size is one.

Besides the molecule in insulator we can imagine a molecule linked direcly to the electrodes. Also in this case we can simulate the junction by a barrier. The angular dependence described by the term β can be motivated in the same way asi in [3].

In the following sections we will present various parametric regimes of our model. We will make the approximations suitable for particular choices of parameters and simultaneously we will compare them with the results obtained from the exact model presented in the previous chapter. Before we do so, let us discuss the influence of the free parameters and suggest interesting parametric regimes.

The behaviour of the model depends relatively strongly on the moment of inertia I (and therefore on the mass) of the bridging molecule. Thus we will first study the transmission probability as a function of energy E for I big enough, namely for $I \geq 100$, which reasonably well corresponds to a real molecule. In this case it is hard to excite the junction hence the problem can be for particular angles φ described by the one-dimensional model and the overall behaviour matches very well the *Chase approximation* [7]. More interesting model we naturally obtain for $I \in (1, 100)$ when the vibrational degree of freedom becomes more evident. On that account we will focus mainly on this case.

Further dividing of the parametric regimes is given by the constants determining the height of the potential barriers. The parameter α indicates the mean strength of the barriers, which is inversely proportional to the coupling between the molecule and continuum. This fact is quite intuitive because naturally if we strenghten the potential then the transmission probability is smaller and hence

the interaction with the molecule is also less probable. The parameter α therefore separates the *resonant transport* (in the case of weak coupling) from the *balistic transport* (strong coupling). The parameter β characterizes the inelasticity of the problem. If we set $\beta = 0$ the problem divides into two parts - to mutually noninteracting electron and vibrations. Hence, the wave function can be written as the product of electronic and vibrational wave function and the vibrational state does not change during the scattering process. Consequently, for small values of β the model does not depend on angle φ that much, whereas for β bigger the internal degree of freedom is nonnegligible. In other words, the parameter β indicates the strenght of the vibrational coupling.

Concerning the parameters α and β we will study the following regimes. First, if both the costants are small then the Chase approximation works because the excitation of vibrations is weak. The smallness of α depends also on the size of I. Next regime we will focus on is characterized by α big and several times greater than β. The model with similar settings can be well described by the *LCP approximation* of the *projection operator approach* [8] which we will introduce later in this chapter. In this case the transmission probability is characterized by narrow peaks and the capture of the electron to the resonant state is responsible for the vibrational excitation. Eventually, if we choose β roughly as big as α or even bigger we can use either the full model or the projection operator approach including the energy dependence, that is without the LCP approximation. In addition, if the moment of inertia I is very small even the projection operator approach fails since the *Born-Openheimer approximation* cannot be used. It is hard to specify what the "small I" means here, nevertheless, from the LCP approximation results below we will see that for $I = 5$ it still works.

The dependence of the transmission probability on the relative orientation φ_0 of the barriers is more apparent for significantly inelastic regimes when we choose β bigger than α. We will illustrate this case at the end of this chapter.

3.1 Elastic approximations and corresponding parametric regimes

We start with the description of the elastic part of the scattering contained in our problem, which is the more trivial part of the model. At first we will neglect the φ-dependence of the problem and we will substitute the angular dependent barriers by fixed barriers with average height (this approximation is accurate for $\beta = 0$). That means we will be interested just in the overall behaviour of the full model comparing it with the simple double delta potential barrier from the first chapter.

After that we will investigate the full problem in regimes with big I when the rotational movement is slow and the electron scatters so quickly that the rotational coordinate almost do not change during the scattering process. Hence, this case is well described by one-dimensional model with coordinate φ set to a certain value. We will study these dependences and eventually we will proceed to the Chase approximation which can be computed by averaging of the transmission probabilities for various angles φ.

3.1.1 1D approximation

Given the parameter β is set to be zero then the initial vibrational state of the system cannot be changed and it holds $m_{in} = m_{out}$. Hence, we obtain a problem analogous to the electron scattering off two fixed delta function potential barriers spaced by $2a$ which we discussed in the first chapter. For the $P_T(E)$ dependence we would again obtain the same curve as is depicted in Figure 1.1.

When the φ-depending potential terms of the barrier are turned on the $P_T(E)$ curve changes. The transmission probability dependence for the case when $\alpha = 1$ and $\beta = 1$ can be seen in the 3.1 (the blue dashed curve). The relative orientation φ_0 is set to 0.5 rad and the moment of inertia is $I = 100$. This settings of parameters we will use as default within this section. If we use different values of parameters we will mention them explicitly in the discussion of the particular graph.

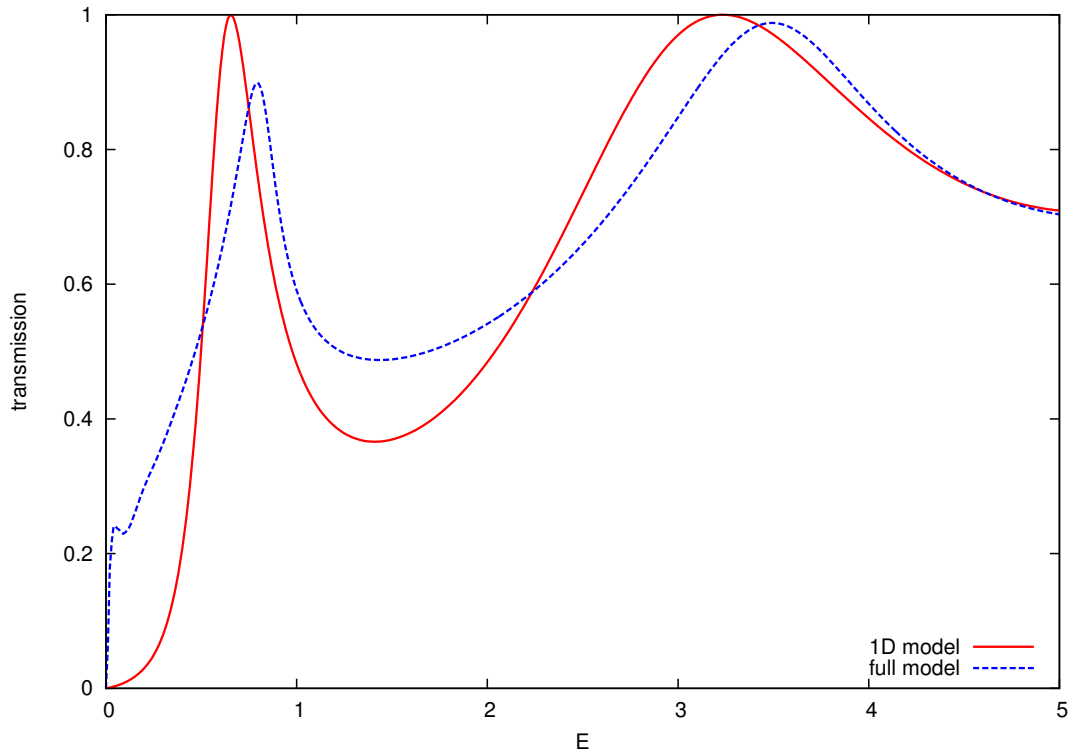

Figure 3.1: This graph illustrates the change in the transmission probability as a function of total energy E which is caused by turning on the rotational delta function potential barriers. The solid curve corresponds to the 1D model with $\alpha_L = \alpha_R = 1$. The dashed curve represents the $P_T(E)$ dependence for the full model considering the rotational delta function barriers have the same height as the fixed ones and their height is small, namely $\alpha = \beta = 1$. The orientation of the barriers φ_0 is 0.5 rad, the molecular moment of inertia is $I = 100$ (default settings).

Comparing the curves in Figure 3.1 it is obvious that both peaks of the 2D solution with β nonzero (the blue dashed curve) are lower and slightly shifted than those in the simple one-dimensional case ($\beta = 0$) which is represented by the red solid curve. The decrease of the peaks is caused by two facts. The first is that by setting the parameter β to a nonzero value we have included the internal

degree of freedom to the model and the second is that the double barrier became asymmetric (the left barrier does not change synchronously with the right barrier because the mutual orientation of the rotational barriers φ_0 is not zero). The fact that the asymmetry of the double barrier causes the decrease of the resonance peaks was demonstrated in the first chapter in Fig. 1.2. No bigger modification of the resonances occurs. However, at the beginning of the graph we can see a new subtle structure which is caused by a threshold effect. Since it appears exactly at the energy $E = \frac{3^2}{2I} = 0.045$ it probably corresponds to the opening of the channel $m = 3$.

We could plot also the reflection probability as a function of energy but it would not give us more information, the graph would be just turned upside down because the condition $P_T + P_R = 1$ must be satisfied.

To make the one-dimensional approximation we can directly employ the results P_T and P_R from the first chapter, we just have to replace constants α_L, α_R by terms $\lambda_L(\varphi) = \alpha_L + \beta_L \cos(\varphi)$ and $\lambda_R(\varphi) = \alpha_R + \beta_R \cos(\varphi - \varphi_0)$. Thus we get the transmission probability dependent on $k = \sqrt{2E}$ and the parameter φ

$$P_T(\varphi) = \left| \frac{1}{k^2 + ik(\lambda_L(\varphi) + \lambda_R(\varphi)) - \lambda_L(\varphi)\lambda_R(\varphi)(1 - e^{4ika})} \right|^2 . \qquad (3.1)$$

This expression we can plot as a 3D graph with two independent variables $E = \frac{k^2}{2}$ and φ, see the left graph of Fig. 3.2. Again we set all the parameters of the barrier to the default values. The figure demonstrates the one-dimensional elastic scattering for every possible value of φ. The height of whole barriers (the

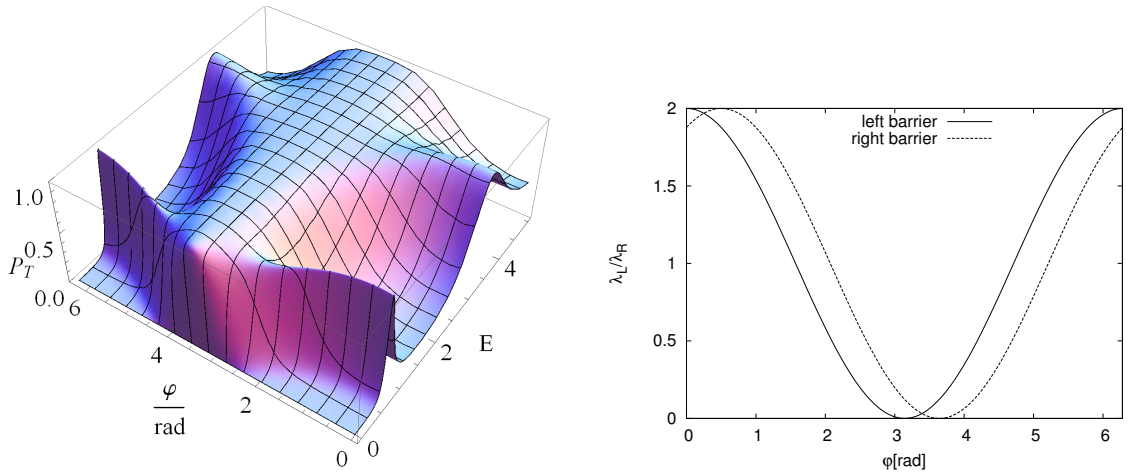

Figure 3.2: In the left figure there is the 3D plot of the transmission probability of the electron through the double barrier as a function of $E = \frac{k^2}{2}$ and φ. The internal degree of freedom is in this case neglected, the graph represents the one-dimensional, elastic approximation of our problem in dependence on φ. The figure on the right describes the heights λ_L, λ_R of both barriers for $\varphi \in (0, 2\pi)$. Parameters characterizing the barriers are set to the default values.

rotational term together with the fixed one) varies with φ as shown in the right graph of Fig. 3.2. We can see that changing the heights of the barriers causes the movement of resonances which in result creates the curved shape of peaks and valleys of the 3D graph. Both graphs are obviously symmetric with respect

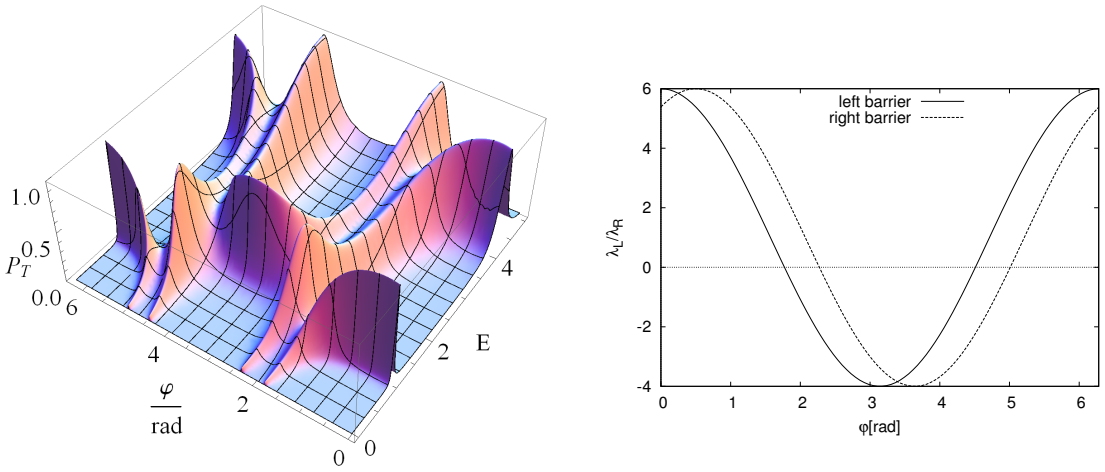

Figure 3.3: The same pair of graphs as above but the parameters determining the height of the barriers now have the following values: $\alpha = 1$, $\beta = 5$. Other parameters have the default values.

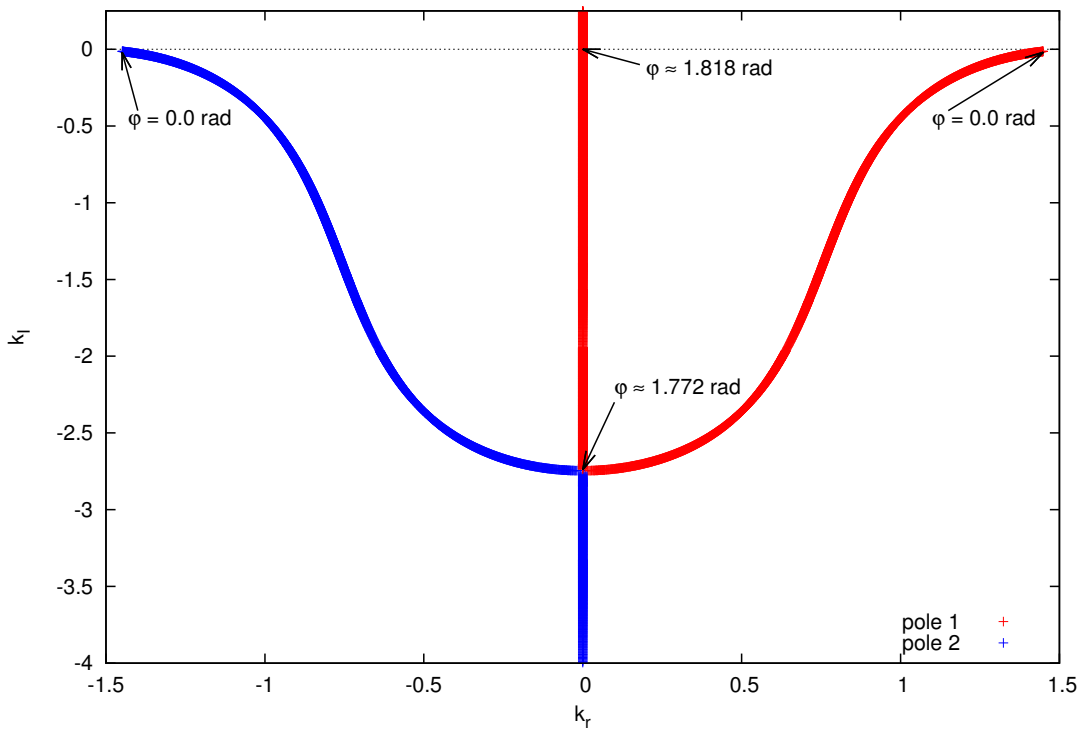

Figure 3.4: In this graph we depicted in red the trajectory of the pole associated with the curved narrow resonance peak closest to the coordinate origin in the 3D graph 3.3 and the blue path corresponds to the pole with the opposite sign before k_r (these poles are complex conjugates in energy). As seen both poles join at the imaginary axis for $\varphi \approx 1.772$ rad creating virtual states and then one of them continues down the imaginary axis, whereas the other one goes up creating a bound state for $\varphi \approx 1.818$.

to the angles $\frac{\varphi_0}{2}$ and $\pi + \frac{\varphi_0}{2}$ (it means that the values corresponding to $\frac{\varphi_0}{2} \pm \vartheta$ for arbitrary angle ϑ are equal, the same is true for $\pi + \frac{\varphi_0}{2} \pm \vartheta$).

For higher values of β we get even richer structure in the appropriate 3D graph. This fact is illustrated in Fig. 3.3 where $\beta = 5$. However, the exact results for similar strongly resonant regimes are more complicated than these approximations and we will discuss them in short at the end of this chapter.

The behaviour of the resonances with changing φ can be analyzed more precisely exploiting the facts mentioned in the theoretical introduction. As we have already said, resonances correspond to the poles of the S matrix, which in consequence means that we just need to find the roots of the expression in the denominator of the fraction inside the absolute value of 3.1. Finding the roots for many different values of φ we obtain the trajectory of the pole in the complex plane. To get a better physical insight it is convenient to calculate the energy $\tilde{E} = \frac{\tilde{k}^2}{2} = E_r - i\frac{\Gamma}{2}$ corresponding to particular roots $\tilde{k}$. The real part E_r represents the energy of the resonance peak whereas the imaginary part $\frac{\Gamma}{2}$ is its half-width.

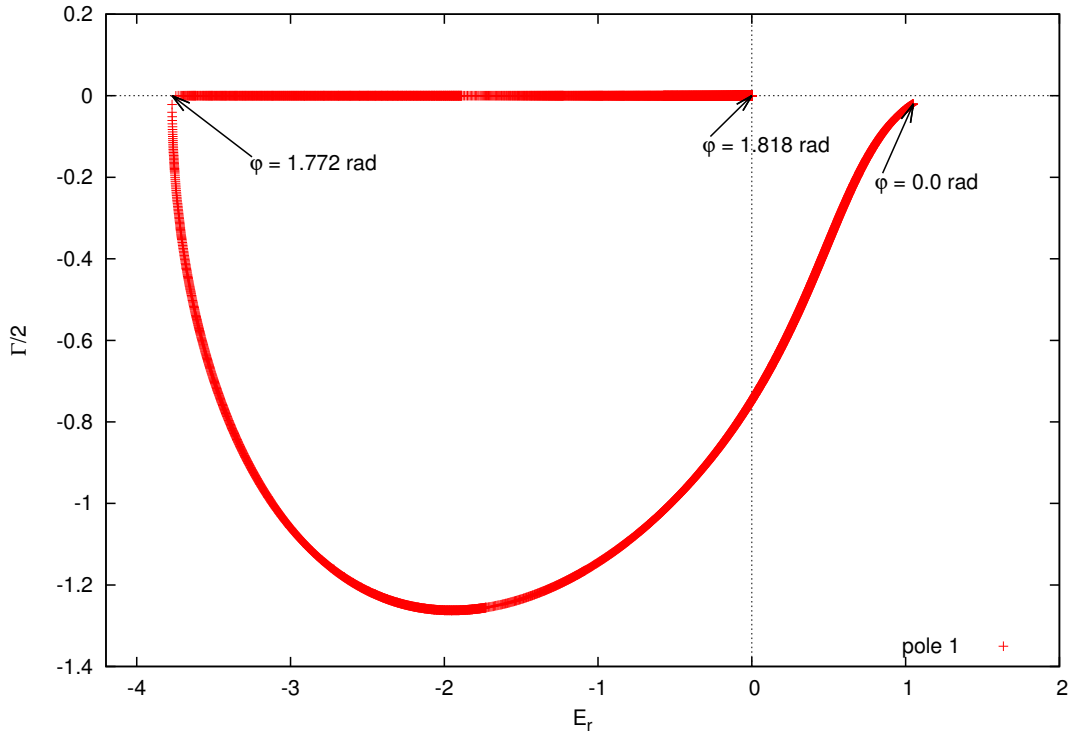

Figure 3.5: This figure illustrates the trajectory of the pole associated with the curved narrow resonance peak closest to the coordinate origin in the 3D graph in Fig. 3.3. The real part E_r of the pole determines the energy at which the peak is located whereas the imaginary part $\frac{\Gamma}{2}$ represents the half-width of the peak.

For the computation of the poles we used the well-known *Newton method* described in [6] which we modified for work with a complex function dependent on a complex variable.

In Figure 3.4 the red path determines the trajectory of the pole associated with the resonance which causes the narrow curved peak in the region $\varphi \in (0, 1.8)$, $E \in (0, 1)$ of the 3D graph 3.3. Blue points represent the path of the pole with the same imaginary part but with negative real wave vector component k_r. These

two poles are in fact complex conjugates in energy. For $\varphi \approx 1.772$ rad both poles join at the imaginary axis creating virtual states. After that, one pole goes down the imaginary axis and the other one moves upwards and approximately for $\varphi \approx 1.818$ rad it crosses the coordinate origin creating a bound state.

If we plot the red resonance path in the energy complex plane we get Fig. 3.5 which enables us to describe the behaviour of the transmission probability in Fig. 3.3. As seen from this 3D graph, for increasing φ the resonance peak in the region $\varphi \in (0, 1.8)$, $E \in (0, 1)$ moves towards zero energy and its width (measured in the energy direction) is getting bigger until the peak completely disappears. This evolution perfectly agrees with the beginning of the movement of the pole in the energy complex plane, see Fig. 3.5. Starting at point corresponding to $\varphi = 0.0$ rad the pole goes to the left towards the imaginary axis (E_r gets smaller) and becomes more distant from the real axis (Γ increases). However, after it crosses the imaginary axis we can no longer find the corresponding resonance peak in Fig. 3.3 because the 3D graph is plotted just for positive values of energy. Further evolution of the pole in the energy complex plane is following: the pole moves across the third quadrant towards the real axis where it becomes a virtual state (for $\varphi \approx 1.772$ rad). Then it follows the real axis to the right, for $\varphi \approx 1.818$ rad it touches the coordinate origin creating a bound state and this bound state moves back to the left following the real axis.

3.1.2 Chase approximation

Although the graph 3.2 represents a good visualisation of the elastic scattering process for particular angles φ, it can be hardly compared with the total transmission probability given by the exact inelastic model. Therefore we integrate the expression 3.1 over φ to get the Chase approximation of the total transmission

$$P_C^T = \frac{1}{2\pi} \int_0^{2\pi} \left| \frac{1}{k^2 + ik(\lambda_L(\varphi) + \lambda_R(\varphi)) - \lambda_L(\varphi)\lambda_R(\varphi)(1 - e^{4ika})} \right|^2 \mathrm{d}\varphi. \qquad (3.2)$$

This process can be understood as averaging of the transmission probability over the angle φ. Hence, particularly the structures significant in the angular direction of the 3D graph 3.2 will be evident in the resulting graph. Obviously, in Fig. 3.2 the main structures can be found around energies $E = 1$ and $E = 3.5$. Therefore the peaks of corresponding Chase approximation will appear also in these regions and their exact positions and widths will be given by the average of the observed structures over φ.

The positions of particular structures are quite expectable because the resulting peaks should always stay close to the energy levels of infinite potential well. Generally, possible energies of the particle in a box are determined by the relation $\frac{n^2\pi^2}{2a^2}$. Hence, for $a = 2$ the energy of the first level is circa 1.2. Apparently, this value really lies in the region of energy $E = 1$ where we observe the first peak.

The Chase approximation in fact contains only the information about the elastic scattering off the delta potential barriers. Therefore it describes very well the weak inelastic regimes of the full model. If we compare the exact results with those given by the Chase approximation we can easily distinguish the nontrivial effects caused by the internal degree of freedom.

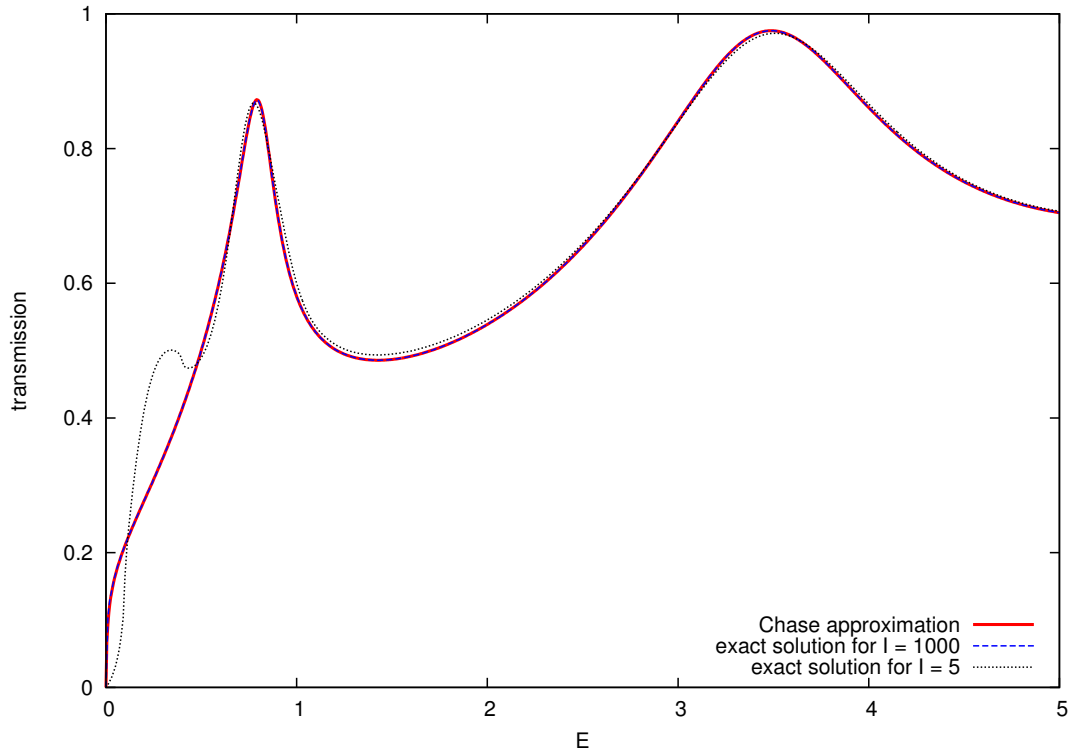

Figure 3.6: The figure above represents the comparison of the exact results obtained from our model with their Chase approximation (the solid curve) given by relation 3.2. The dashed line illustrates the precise solution for $I = 1000$, the dotted curve corresponds to $I = 5$.

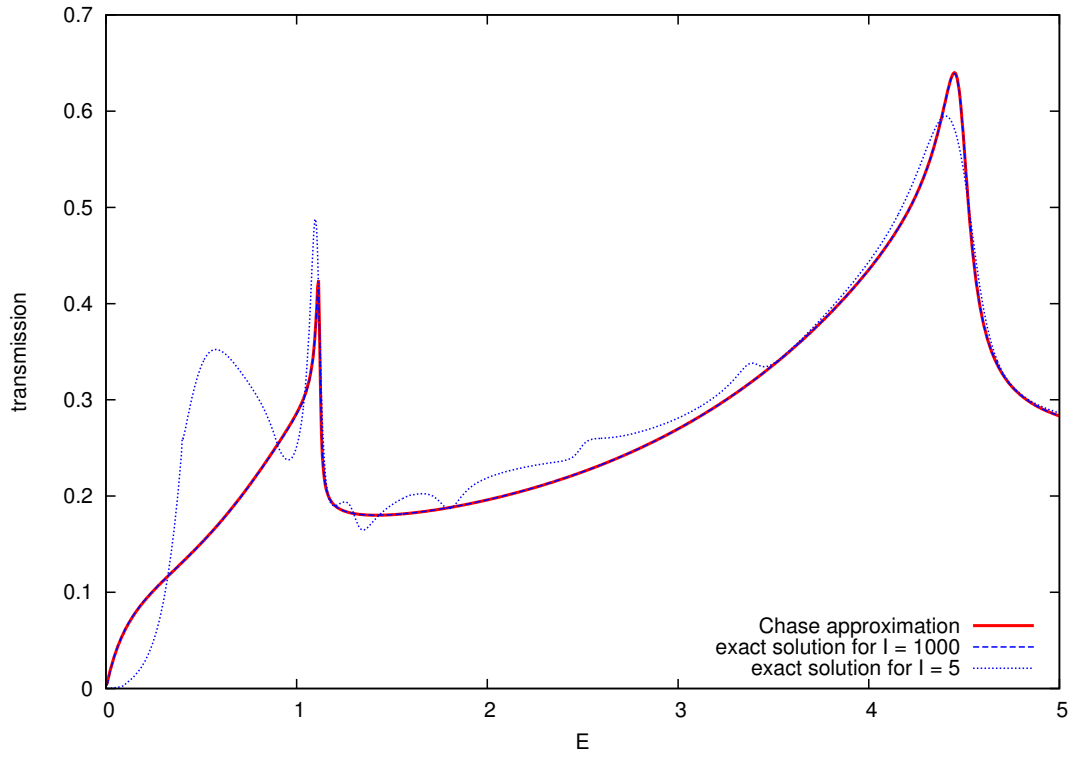

Figure 3.7: This graph illustrates the fact that for big coefficients $\alpha = \beta = 5$ and small I the Chase approximation cannot be used. The orientation of the barriers is $\varphi_0 = 0.5$ rad as usual.

The integral of 3.1 over φ we computed numerically setting the parameters of the barriers again to the default values. Obtained data are plotted together with the corresponding exact solutions in Figure 3.6. As can be seen the exact curve for $I = 1000$ is precisely the same as the approximate one. There are no deviations between the two graphs even for small energies. The dotted curve describes the exact transmission for $I = 5$. This dependence visibly differs from the approximation. The reason is simply the easier excitation of the molecule which in turn causes a change of the electron energy and therefore it also modifies the transmission probability graph. The deviations can be observed particularly in the region of small energies for which the interaction with the vibrational degree of freedom is more probable and where also the threshold effects occur.

If we additionally strenghten the barriers to the value $\alpha = \beta = 5$ the exact solution for small molecular moment of inertia differs from the Chase approximation more, see Fig. 3.7. However, the exact transmission probability for $I = 1000$ coincides with the approximation very well. We can also notice that both peaks again lie nearby the energy levels of infinite potential well. Logically, now they are closer because the average height of the double barrier is bigger.

3.2 Discrete state in continuum

Throughout this section we will discuss the behaviour of another parametric regime of our model. We will investigate in more detail the case when the coefficient α is big and greater than β which is also bigger than 1. Since with similar settings it is much easier to excite the vibrations we will focus especially on the molecular excitation from the ground state $m_i = 0$ to a higher vibrational state m_f applying another approximate approach used in molecular physics. Namely, we will try to describe the narrow resonances appearing in the graphs of transmission probabilities by the *projection operator approach* [8]. This method is commonly used for the study of real molecules.

At first, we will outline the theory associated with this method and we will present the resulting relations. Afterwards we will procceed to the computation based on these results and we will compare the results with transmission probabilities given by the exact solution from the previous chapter.

3.2.1 Theoretical background

As we have already mentioned the cross sections and hence also the transmission probabilities vary rapidly and can attain high values in the neighbourhood of resonance energies when the electron is captured into unstable quasi-bound state. The main point of the approach we are about to use is the fact that near the resonance we can describe the wave function by square integrable function spanning small subspace $\mathcal{Q}$ of the Hilbert space $\mathcal{H}_\mathrm{e}$ incident to the electron. Therefore it is convenient to write the following separation $\mathcal{H}_\mathrm{e} = \mathcal{P} \oplus \mathcal{Q}$ which divides the electronic Hilbert space into the small part $\mathcal{Q}$ containing the most of the resonance wave function and the remaining non-resonant part $\mathcal{P}$ called background scattering. The Hilbert space can be separated employing the projection-operator formalism of Feshbach [9] which we outline in the following paragraphs.

Let us consider the potential scattering problem characterized by the Hamiltonian

$$H_e = \frac{p^2}{2} + V, \tag{3.3}$$

where V denotes an arbitrary local potential. First we introduce the operators P, Q that project on the corresponding parts $\mathcal{P}$ and $\mathcal{Q}$ of the full Hilbert space $\mathcal{H}_e$. These projectors satisfy the relations

$$P^2 = P,\ P^\dagger = P, \tag{3.4}$$

$$Q^2 = Q,\ Q^\dagger = Q, \tag{3.5}$$

$$PQ = 0,\ P + Q = 1. \tag{3.6}$$

Now we decompose the scattering process into resonant and background parts. To do so we start with solving the free particle problem just in the $\mathcal{P}$ space obtaining vectors $|\vec{k}\rangle$. Then one has to find the wave functions $|\phi_k^{(\pm)}\rangle$ describing the electron scattering off the potential V with the constraint $Q|\phi_k^{(\pm)}\rangle = 0$ where $|\phi_k^{(\pm)}\rangle$ are the background scattering wave functions. The final step is to separate into the subspaces $\mathcal{P}$ and $\mathcal{Q}$ the complete scattering wave function $|\psi^{(\pm)}\rangle$ determined by the Lippmann-Schwinger equation

$$|\psi^{(\pm)}\rangle = |\vec{k}\rangle + G_0^{(\pm)} V |\psi^{(\pm)}\rangle,$$

where the ket $|\vec{k}\rangle$ represents the free electron wave function related to the wave vector $\vec{k}$. Whole derivation can be found in more detail for instance in [8]. Currently, we are going to present just the resulting relations important for our approach.

The separation process yields the decomposition of the T matrix into background and resonance parts

$$T(\vec{k}', \vec{k}) = T_{bg}(\vec{k}', \vec{k}) + T_{res}(\vec{k}', \vec{k}), \tag{3.7}$$

the resonance T matrix contains the most of information we are interested in. Generally, it can be expressed in terms of the background scattering wave functions as follows

$$T_{res}(\vec{k}', \vec{k}) = \langle \phi_{k'}^{(-)} | P H_e Q \left[k^2/2 - H_Q - Q H_e P G_{bg}^{(+)}(k) P H_e Q \pm i\eta \right]^{-1} Q H_e P | \phi_k^{(+)} \rangle. \tag{3.8}$$

At this moment we make some important assumptions valid for our problem. The first is that the resonance subspace $\mathcal{Q}$ is spanned just by one state $|\phi_d\rangle$ usually called discrete state. Hence, the appropriate projector reads $Q = |\phi_d\rangle \langle \phi_d|$. In the second place we assume there are no bound states in the background scattering problem, which means that the background scattering states form a complete set in $\mathcal{P}$ thus we can write

$$P = \int |\phi_k^{(\pm)}\rangle \langle \phi_k^{(\pm)}| \mathrm{d}\vec{k}. \tag{3.9}$$

Under the conditions stated above it is useful to introduce certain quantities. The discrete state energy E_d is naturally given by

$$E_d = \langle \phi_d | H_e | \phi_d \rangle. \tag{3.10}$$

Further we define the coupling of the discrete state with continuum $V_{\mathrm{d}\vec{k}}$ and the level-shift operator $F(k)$ as

$$V_{\mathrm{d}\vec{k}} = \langle\phi_d|\, H_e|\phi_k^{(+)}\rangle, \tag{3.11}$$

$$F(k) = \langle\phi_d|\, H_e P G_{bg}^{(+)}(k) P H_e\,|\phi_d\rangle \equiv \Delta(k) - \frac{i}{2}\Gamma(k). \tag{3.12}$$

Using the relation 3.9, the fact that vectors $|\phi_k^{(+)}\rangle$ form the eigenbasis of the operator $G_{bg}^{(+)}$ and the formula $(x+i\eta)^{-1} = \text{v.p.}\frac{1}{x} - i\pi\delta(x)$, it is possible to express the quantities $\Delta(k)$ and $\Gamma(k)$ representing the real and imaginary part of the level-shift operator as

$$\Gamma(k) = 2\pi \int \left|V_{\mathrm{d}\vec{k}}\right|^2 \mathrm{d}\Omega_k, \tag{3.13}$$

$$\Delta(k) = \frac{1}{2\pi}\text{v.p.}\int \frac{\Gamma(k')}{(k-k')}\mathrm{d}k'. \tag{3.14}$$

Applying the defining relations on the expression 3.8 we get

$$T_{res}(\vec{k}',\vec{k}) = V^*_{\mathrm{d}\vec{k}'}\left[k^2/2 - E_d - \Delta(k) + (i/2)\,\Gamma(k)\right]^{-1} V_{\mathrm{d}\vec{k}}. \tag{3.15}$$

We see that the resonant scattering is fully characterized by the quantities E_d and $V_{\mathrm{d}\vec{k}}$.

The integral cross section depends just on E_d and $\Gamma(k)$, the information about the direction included in $V_{\mathrm{d}\vec{k}}$ is not needed. Hence, we can write the resonant total cross section as

$$\sigma_{res} = \frac{4\pi}{k^2}\frac{\left[\Gamma(k)/2\right]^2}{\left[k^2/2 - E_d - \Delta(k)\right]^2 + \left[\Gamma(k)/2\right]^2}. \tag{3.16}$$

Without the k dependance of Γ and Δ this expression represents the well-known *Breit-Wigner resonance formula*.

The separation process can also be performed for the phases δ corresponding to particular eigenvalues of the S matrix (eigenphases) [10]. The decomposition yields the result

$$\delta = \delta_{bg} - \arctan\left[\frac{\Gamma(k)/2}{k^2/2 - E_d - \Delta(k)}\right]. \tag{3.17}$$

3.2.2 Application to our model

Let us now apply the theory outlined above to our problem including the vibrational degree of freedom. We will use the resulting relations in a slightly modified form to study the resonant part of the electron transmission probability and then we will compare the obtained data with the exact solution discussing the differences.

Instead of the direction dependence of the wave vector we will use the subscripts L and R denoting the electrode on which the electron is localized. In fact, these subscripts will represent two possible values of the additional quantum number i which together with the size of k uniquely determines vectors from continuum.

The method of the discrete state in continuum can be used best for a description of narrow resonance peaks which are very well distinguishable from the background scattering. Hence, we will use this approach to approximate the first narrow peak that can be observed near the energy $E = 1$ in the full model with high barriers. However, we will not solve the problem employing the full projection operator approach. We will make the *local complex potential approximation (LCP approximation)* of this approach, which is commonly used in molecular physics.

According to the projection operator approach the transmission probability for the resonant part of our problem is given by the relation

$$P_{res}^{T} = \left| (2\pi i/\sqrt{k_i k_f}) \left\langle m_f \right| V_{dk_f}^{R} \left[E - E_d(\varphi) + \frac{1}{2I}\frac{\partial^2}{\partial\varphi^2} - F(E,\varphi) \right]^{-1} V_{dk_i}^{L} \left| m_i \right\rangle \right|^2, \tag{3.18}$$

where $F(E,\varphi)$ denotes the energy level shift operator and $V_{dk_f}^{R}$, $V_{dk_i}^{L}$ are the discrete-state-continuum coupling terms for the right and the left barrier.

In the LCP approximation we assume that the functions Γ and Δ do not change with energy because the resonance peak is very sharp. Therefore we consider the energy dependence of these quantities to be constant and equal to the values at the energy $E_r(\varphi) \equiv E_d(\varphi) + \Delta_L(E_r,\varphi) + \Delta_R(E_r,\varphi)$ corresponding to the position of the resonance peak. In other words, in our model Γ and Δ will depend only on the angular variable φ, i. e. we assume $\Gamma(\varphi) \equiv \Gamma(E_r(\varphi),\varphi)$, $\Delta(\varphi) \equiv \Delta(E_r(\varphi),\varphi)$. Furthermore, ignoring the complex phase in 3.13 we can write $V_{\mathrm{d}k}^{i}(\varphi) \approx \sqrt{\Gamma_i(\varphi)/2\pi}$, $i = L, R$.

Therefore the transmission and reflection probabilities can be computed using the following expressions (the φ dependence is for lucidity omitted)

$$\begin{aligned} P_{m_f m_i}^{T;res} &= \frac{4\pi^2}{k_i k_f} \left| \left\langle m_f \right| V_{\mathrm{d}\vec{k}_f}^{R} \left[E - E_r + \frac{1}{2I}\frac{\partial^2}{\partial\varphi^2} + \frac{i}{2}\left(\Gamma_L + \Gamma_R\right) \right]^{-1} V_{\mathrm{d}\vec{k}_i}^{L} \left| m_i \right\rangle \right|^2 \\ &= \left| \left\langle m_f \right| \sqrt{\Gamma_R} \left[E - E_r + \frac{1}{2I}\frac{\partial^2}{\partial\varphi^2} + \frac{i}{2}\left(\Gamma_L + \Gamma_R\right) \right]^{-1} \sqrt{\Gamma_L} \left| m_i \right\rangle \right|^2, \end{aligned} \tag{3.19}$$

$$\begin{aligned} P_{m_f m_i}^{R;res} &= \left| \delta_{m_f m_i} - \frac{2\pi i}{\sqrt{k_i k_f}} \left\langle m_f \right| V_{\mathrm{d}\vec{k}_f}^{R} \left[E - E_r + \frac{1}{2I}\frac{\partial^2}{\partial\varphi^2} + \frac{i}{2}\left(\Gamma_L + \Gamma_R\right) \right]^{-1} V_{\mathrm{d}\vec{k}_i}^{L} \left| m_i \right\rangle \right|^2 \\ &= \left| \delta_{m_f m_i} - i \left\langle m_f \right| \sqrt{\Gamma_R} \left[E - E_r + \frac{1}{2I}\frac{\partial^2}{\partial\varphi^2} + \frac{i}{2}\left(\Gamma_L + \Gamma_R\right) \right]^{-1} \sqrt{\Gamma_L} \left| m_i \right\rangle \right|^2. \end{aligned} \tag{3.20}$$

The unknown functions $\Gamma_L(\varphi)$, $\Gamma_R(\varphi)$ and $E_r(\varphi)$ can be determined by fitting the exact relation 3.1 for various values of φ by the expression characterizing the resonance peak

$$P_{fit}^{T} = \frac{\Gamma_L \Gamma_R}{\left(E - E_r\right)^2 + \left(\left(\Gamma_L + \Gamma_R\right)/2\right)^2}. \tag{3.21}$$

We performed this process for the parametric regime characterized by small moment of inertia I and big coefficient α which is greater than β. Namely we

set $I = 5$, $\alpha = 5$ and $\beta = 2$. Such a choice of constants implies that the first resonance peak is narrow and high enough so the LCP approximation works. Additionally, the influence of vibrations is relatively significant because of the small value of I. The orientation of the molecule we set to the value $\varphi_0 = 0.5$ rad.

So far we presented just the total transmission probabilities and their approximations. However, we can study also the probabilities related to particular channels and especially to transitions between them. It means we can compute the probability of the molecular excitation from the ground state to a higher state. Therefore in this section we will focus not only on the total transmission but also on the probability of the molecular excitation from the ground state to the first excited state. In the following graphs we will present the results retrieved for the choice of parameters mentioned above.

In Figure 3.8 we depicted the exact total transmission probability together with the LCP and Chase approximations in the interval $(0, 2)$ where the first narrow resonance peak appears. To see better the subtle resonant structures around the peak we set the logarithmic scale at the y axis. The curve of the LCP approximation matches the main peak of the precise solution very well but the further from this extreme we are the bigger is the difference between the curves. This is

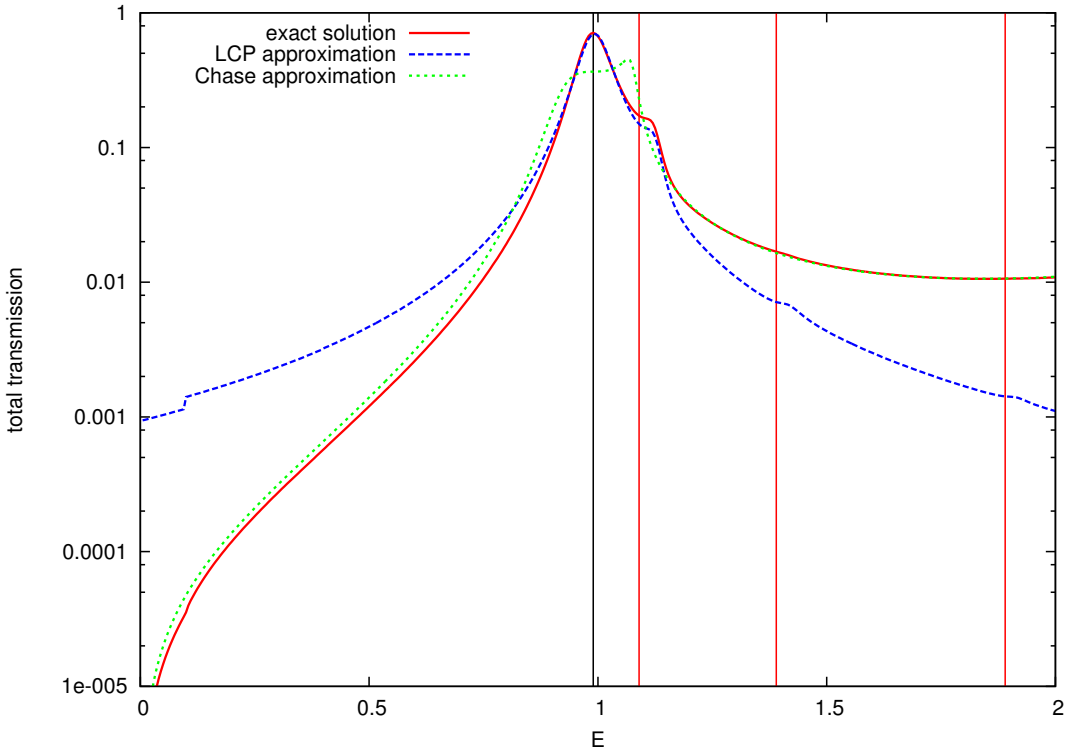

Figure 3.8: The red solid curve of this graph is the exact transmission corresponding to the regime with parameters $I = 5, \alpha = 5$, $\beta = 2$, $\varphi_0 = 0.5$ rad, the blue dashed line represents the LCP approximation of the resonant transmission probability and the green dotted curve is the Chase approximation for the same model. The main resonance peak positioned at energy E_r is marked by the black vertical line, whereas the the red lines indicate the energies $E_r + \frac{m^2}{2I}$ of excited resonant states for $m = 1, 2, 3$.

caused just by the fact that the background part of the scattering is not included in the approximation. On the contrary, the Chase approximation matches the exact solution in the side regions where the background scattering dominates and it differs significantly around the main peak. In the graph we marked the energy corresponding to the main peak by the black vertical line. The three red vertical lines to the right from the black one determine the energy of the main peak plus the vibrational energy $\frac{m^2}{2I}$ gradually for $m = 1, 2$ and 3. Obviously, near each red line we can find a subtle peak of the LCP approximation. These structures can be understood on the basis of relation 3.18. Its denominator is evidently zero for the corresponding energies, which causes the increase of the transmission probability in appropriate regions. The subtle peaks corresponding to $m = 2$ and 3 are visible only in the LCP approximate because in the exact solution they are suppressed by the background scattering and the Chase approximation neglects the vibrational degree of freedom. The little jump of the blue dashed curve at the energy 0.1 is caused by a threshold effect, which is not treated consistently in the LCP approximation.

Now we focus on Fig. 3.9. The red solid curve represents the probability of the electron transmission through the junction without any excitation of the

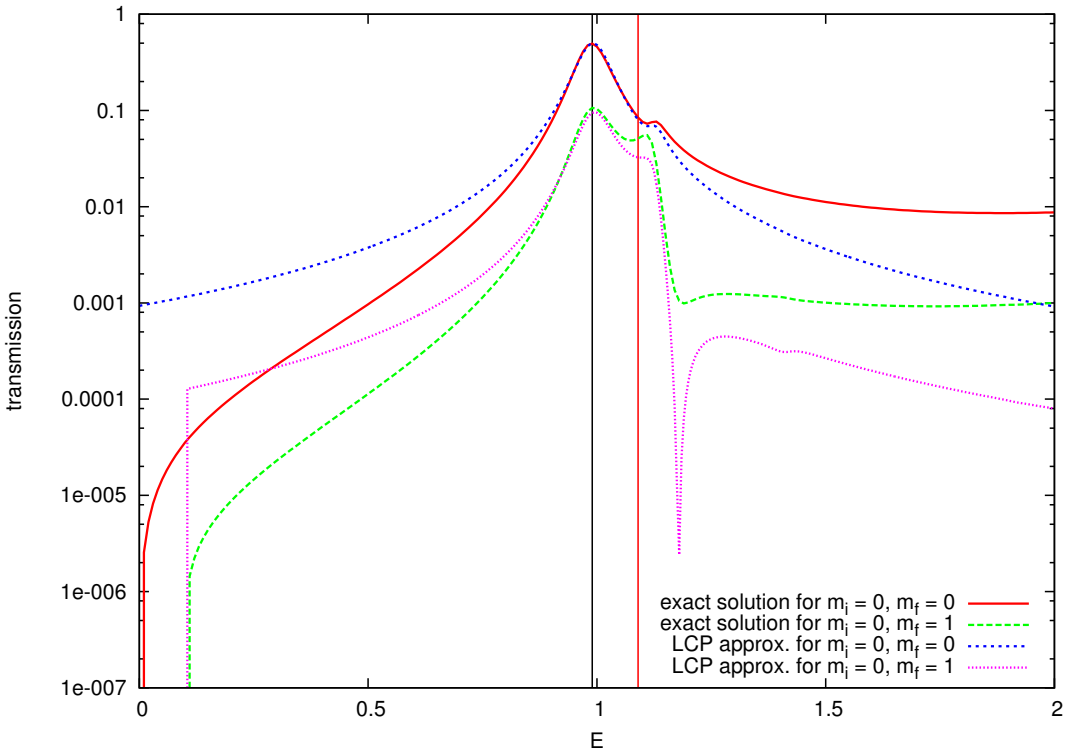

Figure 3.9: In this figure we plotted the transmission probabilities for two different cases: $m_i = 0$, $m_f = 0$ and $m_i = 0$, $m_f = 1$. All the parameters are set to the same values as in the previous graph. The red solid curve represents the probability of the electron tunneling without any molecular excitation, the green dashed line describes the probability of the electron transmission causing the excitation of the junction to the first excited state. Remaining two curves are the LCP approximations of the exact solutions. The energies E_r (black) and $E_r + \frac{1^2}{2I}$ (red) are marked by vertical lines again.

molecule, that is it holds that $m_i = m_f = 0$. The green dashed dependence is the probability that the electron causes the transition from the ground vibrational state ($m = 0$) to the first excited state ($m = 1$). All the parameters characterizing the barriers are the same as in the previous graph. The LCP approximations again coincide well with the exact solutions, the difference between the exact and approximate curves is just the background scattering which is omitted in our approach. The black vertical line indicates the energy E_r of the main peak and the red one denotes the energy $E_r + \frac{1^2}{2I}$ corresponding to the side peak.

The inelastic scattering causes that the electron loses the energy in favour of the molecule. We can determine the vibrational energy of the excited junction computing the mean value of the quantity $\frac{m^2}{2I}$. In our case we can again compare the exact results with the LCP approximation, see Figure 3.10. Evidently, the curves coincide well in the region of the main peak whose position is naturally the same as in the transmission probability graph. The height of the peak reaches approximately the value 0.05. Hence, we see that the excitation of vibrations is small in comparison with the total energy of the system despite the fact that the moment of inertia is set to the value $I = 5$. To achieve a greater vibrational energy we would have to strenghten the vibrational coupling, i.e. the height of the rotational barriers determined by β. However, for such a regime we could not use the LCP approximation.

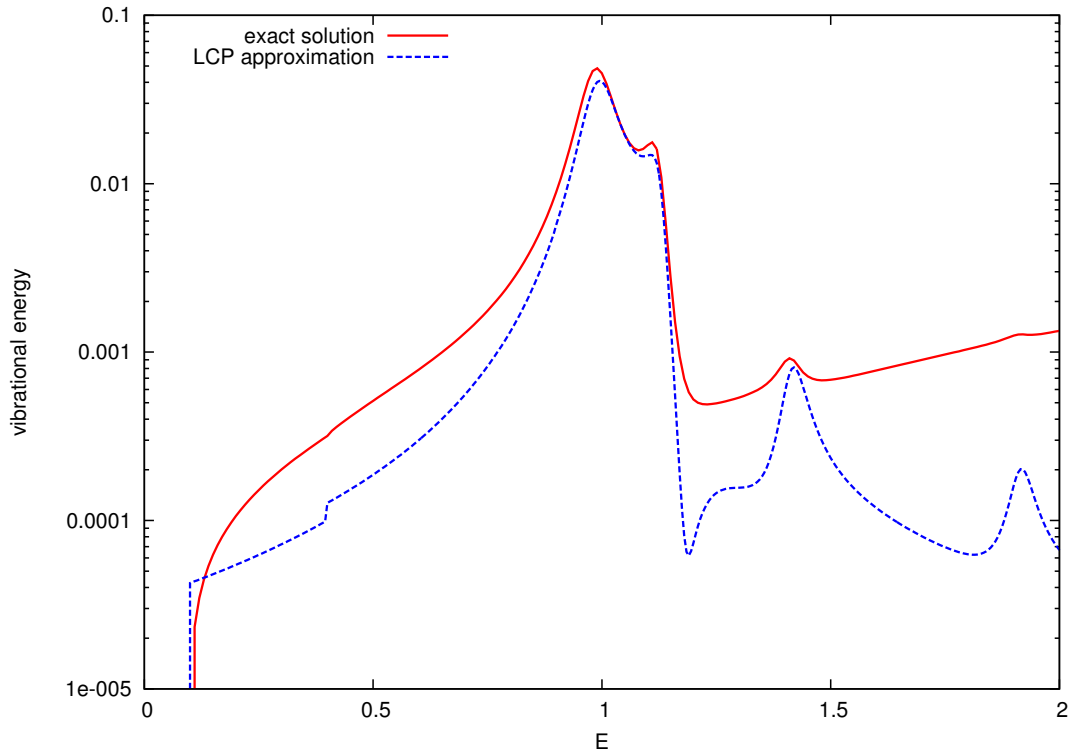

Figure 3.10: This figure illustrates the vibrational energy $\langle \frac{m^2}{2I} \rangle$ as a function of the total energy of the system. The exact solution (red solid curve) is approximated by the LCP approximation (the blue dashed curve).

3.3 Strong coupling regimes

The behaviour of our model changes significantly if we set a small molecular moment of inertia I or when the coefficient β is big and much greater than coefficient α. This fact is reasonable because a small moment of inertia I or a big vibrational coupling implies easier excitation of the molecule. Therefore we can observe many nontrivial inelastic and threshold effects whose explanation can be complicated.

Let us now demonstrate the influence of vibrations on the model behaviour for the parametric regime with a reasonably high moment of inertia but with a strong vibrational coupling. Namely, we focus on the model characterized by the following values of parameters: $I = 100$, $\alpha = 1$ and $\beta = 5$. The transmission probability corresponding to this parametric regime depends significantly on the mutual orientation of the barriers. Therefore we computed it for various values of φ_0, see Figure 3.11 where we depicted the transmissions in the region of energies $(0.0, 2.5)$ which contains the main narrow resonance peak.

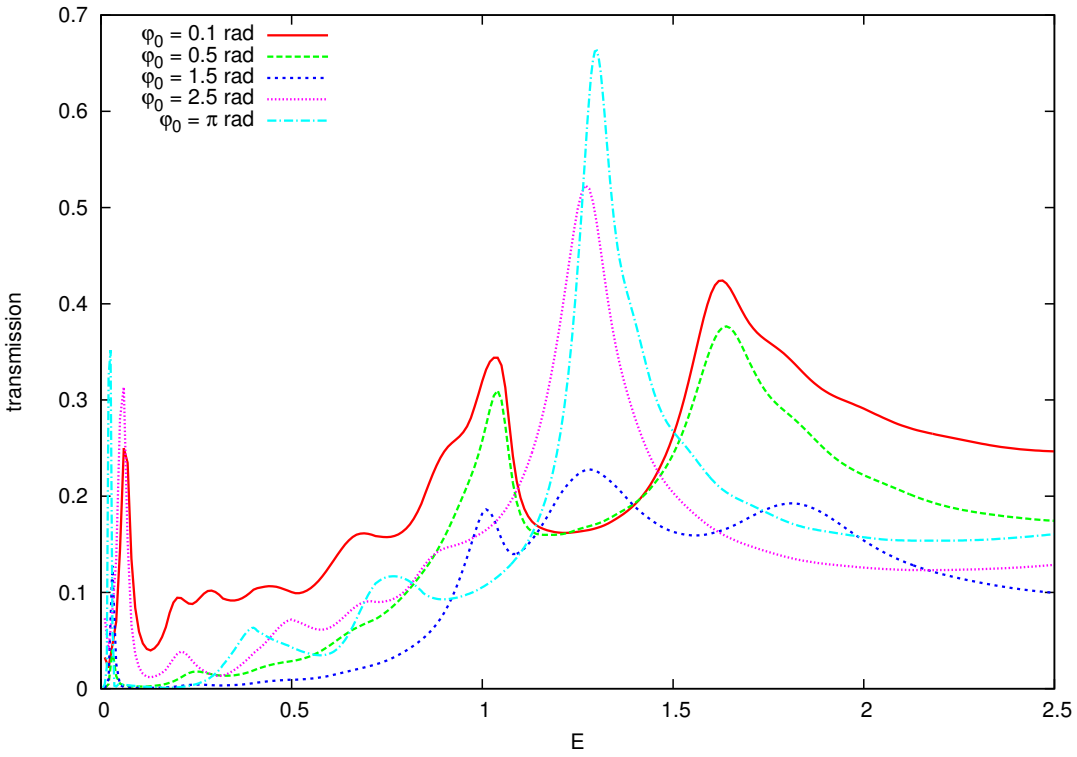

Figure 3.11: Here we compare the transmission probabilities in the region of small energies for various values of φ_0. The height of the barriers is $\alpha = 1$ and $\beta = 5$. The molecular moment of inertia we set to $I = 100$.

As can be seen for φ_0 near to π there is a high and narrow resonance peak in the centre of the figure. When decreasing φ_0 the peak gradually modifies into three subtle wrinkles from which the two outer visibly increase for φ_0 very small. Since the moment of inertia of this regime is quite big we can compare particular curves from Fig. 3.11 with Fig. 3.3 and with similar 3D graphs for different values of φ_0 which are presented below. Focusing on Fig. 3.3 we can see that the resonance structure around energy $E = 1$ is in fact formed by 3 states which move in dependence on φ. However, all of them stay for certain angles in the

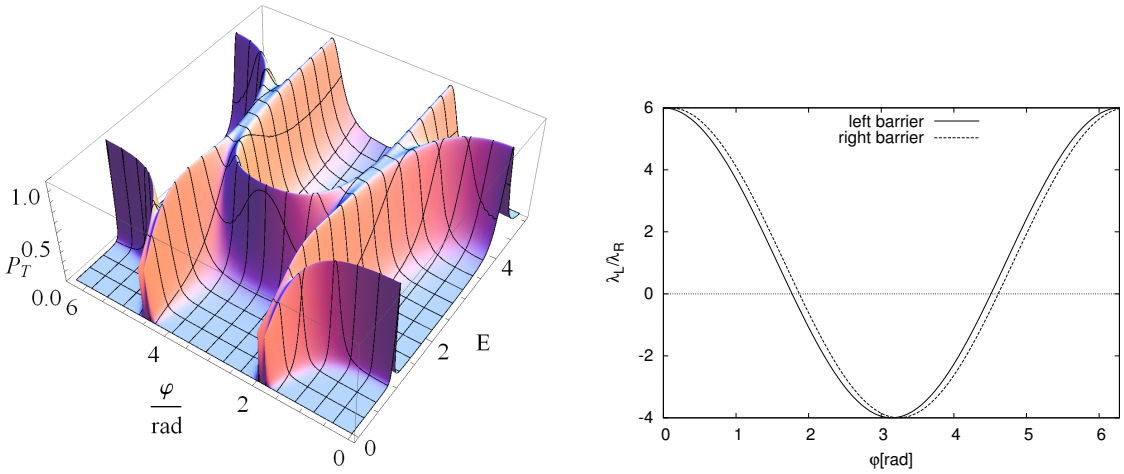

Figure 3.12: Analogous pair of graphs as in Fig. 3.3 for $\varphi_0 = 0.1$ rad.

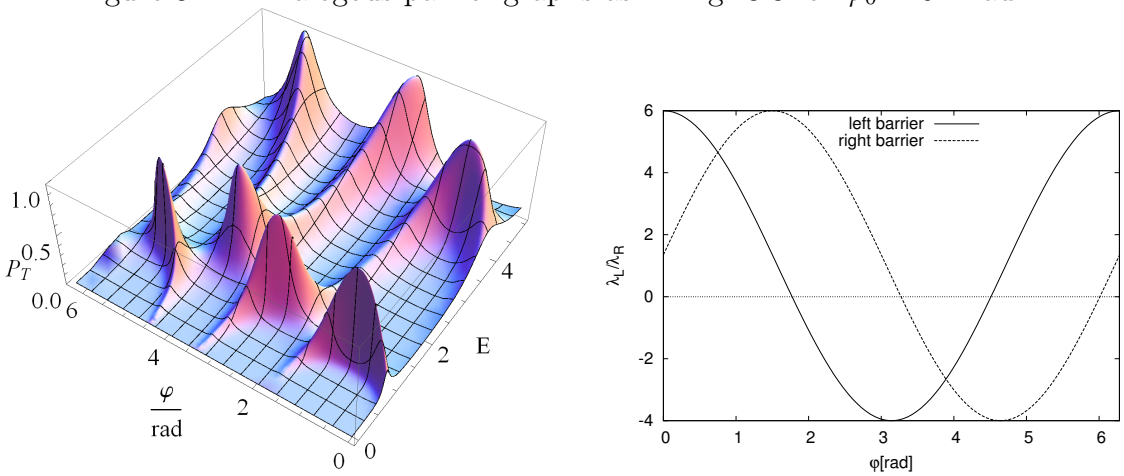

Figure 3.13: Analogous pair of graphs as in Fig. 3.3 for $\varphi_0 = 1.5$ rad.

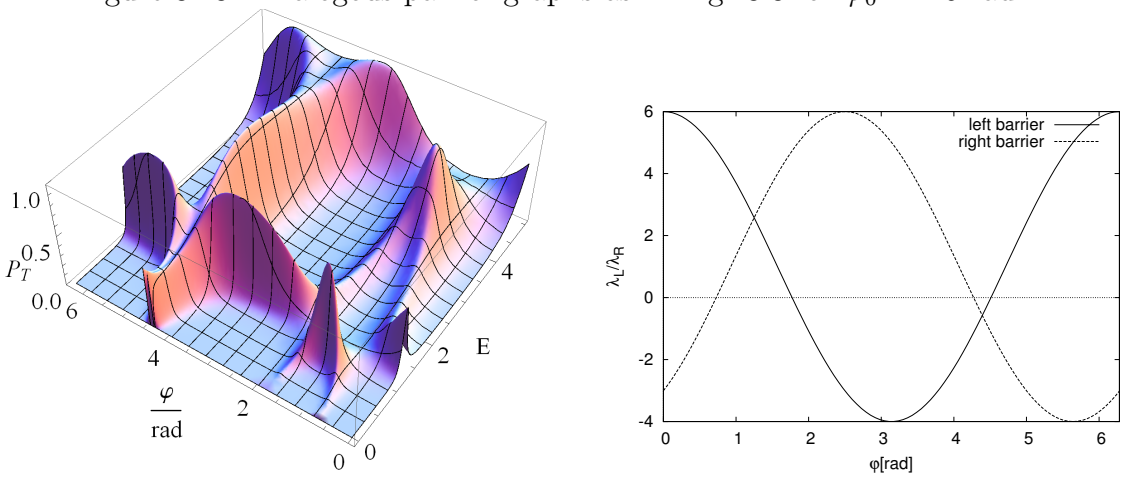

Figure 3.14: Analogous pair of graphs as in Fig. 3.3 for $\varphi_0 = 2.5$ rad.

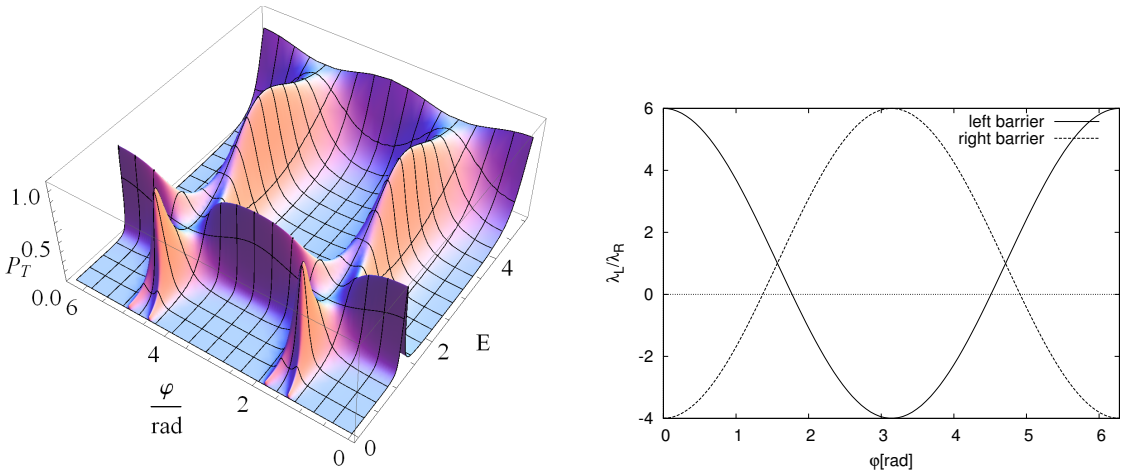

Figure 3.15: Analogous pair of graphs as in Fig. 3.3 for $\varphi_0 = \pi$ rad.

region of energy $E = 1$ whereas other regions they pass over quickly. This quite complicated structure is the reason why we observe more than one main peak in the exact solution with $\varphi_0 = 0.5$ rad. The overall behaviour of other exact curves corresponding to different values of φ_0 can be understood better in context with the 3D graphs in Figures 3.12, 3.13, 3.14 and 3.15.

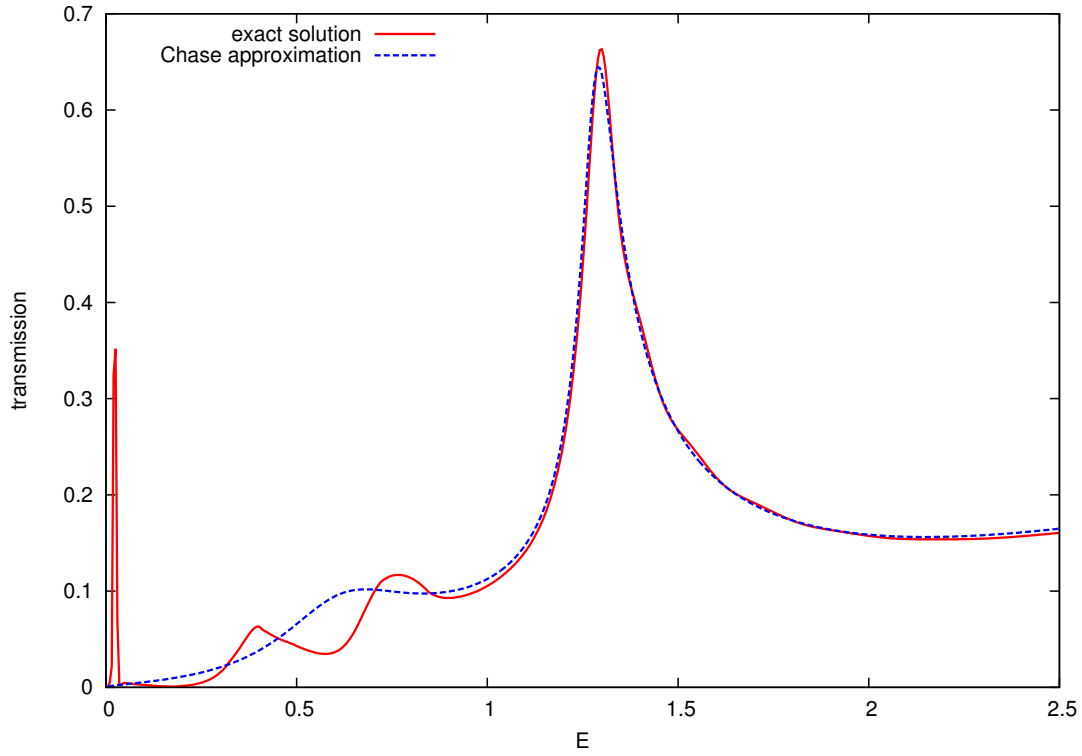

Figure 3.16: Comparison of the exact transmission probability (the red solid curve) for $\alpha = 1$, $\beta = 5$ and $\varphi_0 = \pi$ rad with its Chase approximation (the blue dashed line).

Except for the described elastic behaviour we can observe in Fig. 3.11 also other effects that are caused by the inelasticity of the problem. To distinguish them better it is convenient to compute the corresponding Chase approximation

and compare it with the exact solution. We made this comparison for the solution with $\varphi_0 = \pi$ rad, see Fig. 3.16. Obviously, the biggest difference is the high and very narrow peak which occurs at the very beginning of the curve and which is completely new in comparison with the regimes discussed in previous sections. Additionally, the curves do not match at all for energies smaller than $E = 1$. To understand better the processes involved we would have to solve the problem at least applying the projection operator approach including the energy dependence.

Conclusion

At the conclusion let us sum up the results we have achieved. At first we summarized the principles of scattering theory and applying them to the elementary problem of the double delta function potential barrier we obtained the corresponding transmission and reflection probabilities as functions of energy. Afterwards we focused on the more complicated two dimensional problem of double barrier with anharmonic vibrations. Using the transfer matrix method we found the way how to compute the transmission and reflection probabilities and we outlined the solution of this problem employing scattering theory.

On the basis of the theoretically derived relations we wrote program for the computation of the transmission probability of the electron through the double barrier with anharmonic vibrations. Throughout the second half of the thesis we studied results computed for various parametric regimes comparing them with several approximations. We started with the elastic regimes and the corresponding 1D approximations thanks to which we described the behaviour of the resonance peaks. After that we computed the Chase approximation of certain transmission probabilities. We showed that it agree very well with the exact transmission probabilities corresponding to the elastic regimes with the molecular moment of inertia high enough. Then we investigated the more resonant parametric regimes with much smaller discrete-state-continuum coupling and higher vibrational coupling. We computed the transmission probabilities and the mean vibrational energies employing the full model and we approximated them by the LCP approximation. As supposed this method matched well with the exact graphs in the region of narrow resonance peaks. We also explained the origin of the smaller side peaks occuring in their neighbourhood.

Finally, we presented the exact solutions of the full model for the strong coupling regimes. We compared them with the elastic approximations which helped us to recognize the new structures caused by the strong inelasticity of the problem. To understand them better we would have to use other quantum mechanical methods, which can be the object of further research.

Bibliography

[1] Čížek, M.: *Molekulární elektronika a rezonanční elektronový rozptyl*, Čs. čas. fyz. **55** (2005), 164.

[2] Di Ventra, M.: *Electrical transport in nanoscale systems*, Cambridge University Press (2008).

[3] Pshenichnyuk, I.: *Interaction of electron with vibrating molecules*, Ph.D. thesis, Faculty of Mathematics and Physics, Charles University, Prague (2010).

[4] Ballentine, L. E.: *Quantum mechanics: a modern development*, World Scientific (2010).

[5] Taylor, J. R.: *Scattering theory: the quantum theory on nonrelativistic collisions*, Wiley (1972).

[6] Press, W. H., Teukolsky, S. A., Vetterling, V. T., Flannery, B. P.: *Numerical recipes in Fortran 90: the art of parallel scientific computing*, Cambridge University Press (1996).

[7] Chase, D. M.: *Adiabatic Approximation for Scattering processes*, Phys. Rev. **104** (1956), 838-842.

[8] Domcke, W.: *Projection-operator approach to potential scattering*, Phys. Rev. A **28** (1983), 2777-2791.

[9] Feshbach, H.: *Unified Theory of Nuclear Reactions*, Ann. Phys. (NY) **5** (1958), 357-390.

[10] Čížek, M.: *Resonant processes in atomic collisions*, Ph.D. thesis, Faculty of Mathematics and Physics, Charles University, Prague (2000).